F: ODP3R

Revised Sept/09

The effects of large and small-scale topography upon internal waves and implications for tidally induced mixing in sill regions

By

Jiuxing Xing and Alan M Davies

Proudman Oceanographic Laboratory

Joseph Proudman Building

6 Brownlow Street

Liverpool L3 5DA

U.K.

ABSTRACT

A free surface non-hydrostatic model in cross-sectional form namely two dimensional in the vertical is used to examine the role of larger scale topography, namely sill width and smaller scale topography namely ripples on the sill upon internal wave generation and mixing in sill regions. The present work is set in the context of earlier work, and the wider literature in order to emphasis the problems of simulating mixing in hydrographic models. Highlights from previous calculations, and references to the literature for detail together with new results presented here with smooth and "ripple" topography are used to show that an idealised cross sectional model can reproduce the dominant features found in observations at the Loch Etive sill. Calculations show that on both the short and long time scales the presence of small scale "ripple" topography influence the mixing and associated Richardson number distribution in the sill region. Subsequent calculations in which the position and form of the small scale sill topography is varied, show for the first time that it is the small scale topography near the sill crest that is particularly important in enhancing mid-water mixing on the lee side of the sill. Both short term and longer term calculations with a reduced sill width, and associated time series, show that as the sill width is reduced the non-linear response of the system increases. In addition Richardson number plots show that the region of critical Richardson number, and hence enhanced mixing increases with time and a reduction in sill width. Calculations in which buoyancy frequency N varies through the vertical show that buoyancy frequency close to the top of the sill is primarily controlling mixing rather than its mean value. Hence a Froude number based on sill depth and local N is the critical parameter, rather than one based on total depth and mean N.

1. INTRODUCTION

The extent to which large scale forcing of meteorological or barotropic tidal origin is converted to small scale mixing (e.g. Rippeth et al 2005, Zhai et al 2005, Xing and Davies 2005) is an important topic in physical oceanography as it influences various vertical exchange processes. In addition the problem of determining the extent to which topography in stratified regions influences the degree to which barotropic tidal energy is partitioned between internal waves and mixing has recently been recognised as an important issue in large scale ocean circulation modelling (Saenko 2006, Saenko and Merrifield 2005, Spall, 2001). In shelf edge regions where the density surfaces intersect the shelf slope and there is an appreciable barotropic tide, then a significant baroclinic tide with associated mixing is generated (e.g. New and Pingree 1990, Legg and Adcroft 2003, Baines 1995, Vlasenko et al. 2005, Xing and Davies 1998, 1999, Van Haren 2006). Since the shelf edge is the lateral boundary of the ocean, enhanced mixing in this region might be expected to influence the oceanic circulation and hence climate (Saenko and Merrifield 2005). Recently ocean model simulations have been performed with enhanced mixing in the lateral boundary and have shown that shelf edge mixing has an important influence on the ocean circulation (Spall 2001). Consequently a detailed knowledge of the conversion of barotropic tidal energy into mixing in regions of steep topography and how this is influenced by both large-scale topographic features and small-scale roughness (namely small scale undulations “ripples” on larger scale topography) is important in determining what controls boundary layer mixing.

In parallel with shelf edge work, the extent to which sill topography at the entrance to fjords (e.g. Stigebrandt 1999, Stigebrandt and Aure 1989, Vlasenko et al. 2002) or Lochs (Inall et al. 2004, 2005, Stashchuk et al. 2007) gives rise to mixing in the sill region has been a recent research topic. In these environments the geographical extent of the problem is significantly reduced compared with the shelf edge region. Consequently more detailed

measurements and finer scale modelling is possible. By this means the role of small-scale topographic variations ("ripples") in sill regions (e.g. Klymak and Gregg 2001) can be examined in detail giving insight as to the importance of small-scale topography in seabank areas (e.g. Nash and Moum 2001, Dewey et al. 2005) and shelf edge regions (e.g. Jeans and Sherwin 2001).

Previous high resolution numerical modelling and measurements of the Loch Etive sill region (Inall et al. 2004, 2005) showed (Xing and Davies 2007, hereafter XD07) that it was essential to retain the non-hydrostatic effects within these models in order to calculate vertical mixing. Subsequently, Davies and Xing (2007)(hereafter DX07) showed that a cross sectional model could reproduce the major features of the observed flow and lee wave activity in the region. In addition a cross-sectionally averaged model of Loch Etive, incorporating realistic topography was shown (Stashchuk et al., 2007) to reproduce the internal wave field and flow in the region. Although these cross sectional models cannot include horizontal vortices which contribute to the mixing, these earlier calculations suggest that they can account for mixing produced by non-linear and non-hydrostatic effects. In theory by using turbulence energy models (Mellor and Yamada 1982) to compute sub-grid scale mixing then coarse grid hydrostatic models including such a parameterisation will take account of some of the small scale non-hydrostatic processes that are responsible for mixing. However, in order to avoid such parameterizations, and approximations that can give erroneous mixing, fully non-linear, non-hydrostatic models such as the one used here are required. In addition in order to ensure that such models can accurately reproduce small scale mixing, direct numerical simulations on extremely fine grids (resolutions of order 0.001 m or less) with values of molecular viscosity and diffusivity are required. In practice with present computing power such calculations would be restricted to very small domains (of order tens of metres). Even if such calculations were possible detailed topography on this scale is not

known, and as will be shown here is required if mixing is to be accurately computed. Recently Afanasyev and Peltier (2001) carried out some detailed simulations of flow in Knight Inlet using a mesh of order 1m. Although this grid is fine it is significantly larger than the grids of order 0.001m commonly used in direct simulations of tank experiments, but is the highest resolution that is practical in oceanographic calculations. However such simulations and those presented here cannot resolve Kelvin-Helmholtz instabilities which have to be parameterized together with any other unresolved motion by using background values of viscosity and diffusivity. The assumption here is that a sufficiently fine grid non-hydrostatic model should contain sufficient physics to examine to what extent changes in topography influence the internal wave field and mixing. However, as suggested by Cummins (2000) and discussed in Farmer and Armi (2001), a model that aims to simulate flow in a sill region must be able to accuately represent the bottom boundary layer. As our aim is not to simulate flows in sill regions since this would require a very high resolution three dimensional model, but rather to examine the influence of topography, we think the present model is adequate for this more limited problem.

In view of this earlier work, in order to examine how small and large scale topography influences the flow, the associated internal wave field together with mixing in the region of a sill, it is necessary to use as fine a grid as possible with small background viscosities and diffusivities in order to obtain a stable solution. Calculations (Berntsen et al. 2008) showed that for the problems considered here, and the grid resolution used in the model (see next section) the solution had converged with respect to the grid. However, this does not mean that the model can accurately reproduce the mixing, but that it can give insight as to how this mixing is influenced by changes in both large and small scale topography, that can be accurately resolved on the grid. As the calculations will show, small scale topography does significantly influence the mixing, and hence in any model aimed at accurately reproducing

the mixing it is essential to include this small scale topography which at present is ignored in models of mixing in sill regions. In addition since this small scale topography has an important influence on mixing, it needs to be measured in addition to measuring mixing, if comprehensive data sets for modal validation are to become available. One problem here is that mixing in the region of sills is truly three dimensional, with horizontal vortices and across channel variations in topography playing an important role. This suggests that in any model validation exercise it will be necessary to collect comprehensive data sets in three dimensions rather than just the along channel detailed surveys that are presently performed. In addition calculations will have to be performed using fully three dimensional models using very fine grids, with the associated computational overhead.

Although high resolution models were used by XD07 to examine the influence of sill width upon non hydrostatic effects, no attempt was made to examine in detail its effect or the influence of small scale topography upon this mixing. In short papers, Xing and Davies 2006a, 2006b (hereafter XD06a,b) briefly examined the effect of one form of small scale topography upon sill mixing. Here this earlier work is extended to examine in a more comprehensive way, and bring together these preliminary results. In particular the focus is the role of large and small scale topography in particular the location of small scale topography relative to the sill crest (an effect that has never previously been examined) upon mixing in sill regions. As previously calculations are performed with a non-hydrostatic model in vertical cross sectional form, in essence a two dimensional slice model, with idealized sill topography. A range of sill widths are examined, using initially smooth topography on the lee side of the sill. Subsequently small scale topography with a range of ripple heights and wavelengths is added to the lee side of the topography. In addition the influence of the location of this topography upon mixing is considered. The objective of these calculations is to determine the extent to which large scale and small scale topography influence tidal flow,

the associated internal wave field and mixing in sill regions. By using idealized topography the role of different topographic length scales can be identified.

In terms of the Loch Etive sill, and comparable sills at the entrance to lochs and fjords, the tidal velocity amplitude (U_o) is typically of order 0.5 m s^{-1}, namely an order of magnitude larger than found in the deep ocean. In addition the tidal excursion is about 10km which is substantially larger than sill widths which are usually about 1 to 3 km wide. Typical water depths (h), of order 100 m, are appreciably shallower than those found in the ocean (depths of order 4,000 m), with sill heights (h_o) of order 85 m, occupying a large fraction of the water column, compared to the ocean case. As discussed by Legg and Huijts (2006) there are a number of key parameters which control stratified flow over topography. In particular the Froude number F_r given in Legg and Huijts (2006) as U_o/Nh_o with N buoyancy frequency which as will be shown is significantly larger in the present calculations than in the deep ocean. In addition the relative height of topography h_o/h is again larger than in the ocean. In particular the tidal excursion parameter ($R_L = U_o/\omega L$) with ω tidal frequency and L topographic length scale is appreciably greater than in the deep ocean, due to the larger U_o and smaller L. As R_L increases, so does the non-linearity in the problem, with an increasing tendency for higher harmonics of the tide and unsteady lee waves to be generated. Although Legg and Huijts (2006) examined flow over small scale topography in the deep ocean their parameter range (large h, small h_o/h, and small U_o) is very different to those considered here.

Also in the case of other sills such as Knight Inlet, the tidal excursion is comparable to the sill width (of order 3 km) and hence R_L is significantly lower than the cases considered here where the response to a narrow sill (width of order 1 km) is considered. In essence the present calculations, in particular those with "small scale topography" superimposed on a narrow sill, extends the parameter range beyond that previously considered, and show the importance of small scale topography in enhancing mixing in sill regions.

2. NUMERICAL MODEL

Although a number of non-hydrostatic models exist in the literature (e.g. Lamb (1994), Gerkema (2002), Berntsen and Furnes (2005), Heggelund et al. (2004) as in earlier work (XD06a,b, XD07) calculations were performed using the MIT code, which employs a vertical z coordinate together with a partial cell and a finite volume discretization at the bottom boundary. In the calculations described here, the free surface form of the model was used. As details are given in Marshall et al. 1997a,b, they are not repeated here. In all calculations the model was used in two dimensional (x, z) cross sectional form initially with idealized topography and water depths representing the sill at the entrance to Loch Etive, the location of recent measurements (Inall et al. 2004, 2005). In all calculations motion was induced by barotropic tidal forcing of M_2 tidal period (namely 12.42 hrs) at the western open boundary and a time step dt = 2 s. A Flather type radiation condition was applied for the barotropic tidal input at the open boundary. For the baroclinic motion a flow relaxation zone was used, with the temperature relaxed to its initial value. Such a condition is similar to the sponge layer used by Nakamura et al. (2000). Unfortunately this boundary condition is not ideal, and in limited area domains if long term calculations are performed, some weakly reflected waves can propagate back into the region of interest. For this reason since the domain of the Loch Etive model is small, only short term calculations can be performed before internal wave reflection from the boundaries influence the solution near the sill. Although in the Loch Etive case a detailed study of the generation of internal waves in hydrostatic and non-hydrostatic models has been performed previously (XD07) with DX07, looking at the internal wavefield in the region and a brief indication of the role of small scale topography has been given (XD06a), a more rigorous presentation of the influence of small scale topography upon the internal wave field has never been considered and is given here. Also its role upon the mixing which was not presented in XD06a is given here and discussed

in detail. However, in order to examine these processes in more detail and to perform power spectral analysis in subsequent calculations symmetric sills of varying width and including small scale topographic effects were used. In addition to examine the energy cascade from long period to short period motion, longer time integrations were performed requiring the use of a larger domain. Although some of this work was briefly presented in a short note (XD06b), a more comprehensive report, including new results, particularly those that show how small scale topography near the sill top influence Richardson number distribution and mixing for the first time are given here.

Considering initially the loch problem, where water depths, loch length and sill width (Fig. 1) were taken to approximate those of Loch Etive. However, the topography was much simpler than in Loch Etive where there were a number of sills within the Loch which narrowed towards its head. As details of the Loch Etive topography are shown in Inall et al. 2004, 2005, they will not be repeated here. Since in this paper the main focus is to examine how small scale features of the topography that are often not measured with any degree of accuracy influence the solution, both idealized large scale and small scale topography will be used to gain insight as to the role of the topography. Consequently no direct comparison with Inall et al 2004, 2005 can be made. In addition no detailed discussion of the time evolution of the flow, or how the internal wave field compares with measurements will be presented here, as these topics are covered in XD07. Here the focus is on the role of how topography affects mixing, and as such, the dimensions of the large and small scale topographic features ("ripples") used in the calculations are relevant to modelling loch and fjord regions and measurements within them.

In all calculations, a fine uniform grid resolution dz = 1 m was used in the vertical with the horizontal grid gradually varying from dx = 10 m in the sill region to 100 m outside this area. These grid resolutions were chosen based upon a convergence study of the

influence of grid resolution upon model accuracy (Berntsen et al. 2008). This study showed that the dominant features of the internal flow and wave field could be accurately resolved with such a grid. In addition the grid could accurately represent small scale changes in topography which are usually measured with a coarser resolution. By using such a high resolution grid, artificial/numerical viscosity and diffusion could be kept to a minimum, unlike in conventional shallow sea models with grids of order kilometres. Obviously this could not remove all artificial viscosity and diffusion which arises due to the finite difference form of the equations used to represent the hydrodynamic equations. To effectively remove these, as discussed previously grid scales of the order of 0.001m would be required, or the hydrodynamic equations solved using a spectral approach with a large (of order 1000) number of functions. Naturally both of these approaches would yield a computationally impractical calculation. However by using the present high resolution grid it is possible to minimise artificial viscosity and diffusivity and to examine to what extent changes in topography, in particular the addition of "ripple topography" changes small scale features of the flow and influences mixing. However, as discussed previously mixing is in reality a three dimensional process, and hence cross channel variations in topography will also have a contribution. Hence with such a fine grid in order to avoid artificial smoothing of the solution by using high background diffusion and viscosity coefficients, the coefficients of vertical and horizontal viscosity were set at $A_V = 10^{-3}$ m^2 s^{-1}, $A_h = 10^{-1}$ m^2 s^{-1}, with corresponding diffusivities of $K_V = K_h = 10^{-7}$ m^2 s^{-1} in essence set at molecular levels. Although the choice of these coefficients is to a certain extent arbitrary, they are significantly smaller than those used in conventional coarser grid oceanographic models. Also by using the same coefficients in the calculations without and with "ripple topography", the influence of this change in topography can be assessed independently of that due to viscosity and diffusivity.

As shown recently (Scotti et al., (2007), Scotti and Mitran (2008)) if the ratio of horizontal grid size to water depth is of the order of (h/10) then the horizontal grid is sufficiently fine to represent non-hydrostatic flow. In the present case in the sill region namely -2000m to +2000m, dx=10m with h varying from 15m to 100m. Hence near the sill top where there is no slope this criterion is not exactly satisfied, although elsewhere it is. In the "far field" where dx=100m this criterion is violated, but in this region there is no slope and non-hydrostatic effects are not important. In addition in the present calculations the full non-linear, non-hydrostatic equations are being solved in the presence of "rippled topography" a situation more complex than that considered by Scotti and Mitran (2008). However, resolution is an important issue and as discussed above, as fine a grid as possible is really required, and the Scotti et al., (2007) and Scotti and Mitran (2008) criterion is valuable in choosing this grid, although as shown by the convergence study of Berntsen et al (2009) the present grid is sufficiently fine for the problem considered.

A no heat flux boundary condition was applied at sea surface and sea bed, together with a zero surface stress condition and a quadratic friction law at the sea bed, with drag coefficient k = 0.0025, a typical shallow sea value.

3. INFLUENCE OF TOPOGRAPHY (LOCH ETIVE SILL)

The topography of the region (Fig. 1) is characterized by a constant water depth at the western end of the domain (h = 50 m) with an open boundary at x = -6500 m. The sill is situated at x = 0, with a sill water depth h_s = 15 m, with water depths increasing to h = 100 m on the eastern side of the sill, corresponding to a constant depth basin closed at its eastern end (x = 15000 m). Initial conditions consisted of a horizontal uniform temperature field, with a linear vertical temperature gradient giving a constant buoyancy frequency (N). Initial conditions at time t = 0, of zero horizontal along loch velocity (u) and vertical (w) velocity were specified. Motion was induced by barotropic tidal forcing of the form

$$U = U_o \sin(\omega t),$$

applied at the open boundary. Here U_o is the specified amplitude of the tidal current, at the M_2 frequency ω. At the open boundary the temperature field was relaxed to its initial value. The Coriolis parameter f was fixed at 1.2×10^{-4} s^{-1}, an appropriate value for Loch Etive. As in all cross sectional models with non zero f, a cross loch velocity v which is initially zero is generated. However, the two dimensional cross sectional form means that all derivatives in y direction are set to zero. This form of the model is common to all vertical slice models of lochs and fjords (see Vlasenko et al. (2005), Stashchuk et al. (2007) and references therein for more detail). To determine the influence of small scale topography upon mixing in the sill region, calculations were performed initially (Calc 1, Table 1) with the smooth topography shown in Fig. 1, and subsequently with additional rough/rippled small scale topography (Calc 2, Table 1), on the steep side of the sill. By placing rippled small scale topography on one side of the sill rather than both, its local effect (namely changes in the region of topography) can be separated from its "far field" effect, namely changes on the other side of the sill.

3.1 Solution with smooth topography (Calc 1)

As the dominant aspects of the tidal flow over the sill are discussed in XD07 and XD06a, they will not be presented here. Rather we will concentrate on the new aspects of the work, namely, the influence of both the short (first tidal cycle) (not considered in XD07, XD06a,b, although as we will show important in determining how small scale topography influences the solution) and longer (subsequent cycle) term effects of topography. These effects were examined in an initial series of calculations (Calcs 1 and 2) Table 1. In these calculations $U_o = 0.3$ m s^{-1} and a constant vertical temperature gradient chosen such that $N = 0.01$ s^{-1} were used.

Initially $t = 1/8T$ (where T is the M_2 tidal period) as the flow over the sill increases, downwelling occurs on the lee side and lee waves are generated (see XD07 for a detailed

discussion of the generation of these lee waves). These lee waves are advected downstream by the tidal current as shown in the temperature contours at t = 2/8T, (Fig. 2a). Associated with these lee waves are small scale changes in vertical (w) and horizontal (u) velocity (Fig. 2a) and density inversion cells due to internal wave breaking in the surface layer (Fig. 2a), which subsequently produce significant vertical mixing in the upper part of the water column. In addition there is a downslope jet on the right hand side of the sill which also produces enhanced mixing on the lee side of the sill. (see XD07 for a detailed discussion of the physics of this jet separation). Shear instabilities associated with this jet and the downslope density field together with regions of density inversion give rise to mixing in the sill region at depth. During the flood stage the local Froude number on top of the sill given by $U\pi/Nh$ is about 12.5, based on local velocity of 0.6 m s^{-1}, N = 0.01 s^{-1} and local depth h = 15 m, and wave breaking and mixing occur (Nakamura et al. 2000, Nakamura and Awaji (2001)). The flow in this region is supercritical. However away from the sill top where the water is deeper, h = 100 m, and velocity U is of order 0.1 m s^{-1}, taking N = 0.01 s^{-1} gives a Froud number away from the sill of order 0.3 which is sub-critical. The two regions are separated by an hydraulic transition.

At the end of a full tidal cycle (t = T) substantial mixing has taken place in the surface layer (Fig. 2b). The extent of this mixing will be quantified at the end of the third tidal cycle. In addition at depth on the right hand side of the sill where the flow separation occurs there is evidence of enhanced mixing at about z = -40 m. Since the second tidal cycle does not start from the same initial conditions as the first then there will be some differences in the solution. However, as will be shown, the basic physical processes in the second cycle are identical to those in the first. As discussed in XD07, and briefly mentioned in XD06a, a qualitative comparison shows that the model can reproduce the main features of the flow and associated mixing found in Loch Etive measurements (Inall et al. 2004, 2005).

Consequently, although a rigorous model validation is not possible, the fact that the model can reproduce the main features of the observed flow and mixing, suggests that changes produced by adding small scale topography will be valid.

At t = 10/8T, namely t = 2/8T into the second tidal cycle, there are differences in the solution (Fig. 3a) compared to the first tidal cycle (Fig. 2a). This arises because some mixing has occurred during the first tidal cycle. Since the initial density field is weaker than before, the lee wave distribution has been modified giving rise to a slightly different u-current field although the major features are comparable. At depth (z = -60 m) the temperature field (Fig. 3a) shows vertical displacements of the isotherms due to lee wave activity. The magnitude of this displacement is about 18 m, and is in good agreement with the 20 m reported by Inall et al. (2004). However, as we will show this is sensitive to small scale features of the topography since the lee wave distribution depends upon the Fourier transform of the topography.

At t = 14/8T there are no substantial differences in the cross sill velocity compared to t = 6/8T, showing that a sinusoidal barotropic tide had been established. However, the well-mixed region on the right hand side of the sill was more extensive than that at t = 6/8T. The enhanced mixing is due to the additional mixing that occurred during the first cycle. At the end of the second cycle it is clear from the temperature contours (Fig. 3b) that the region of enhanced mixing that occurred on the right hand side of the sill at t = 14/8T, has now been advected over the top of the sill. This gives rise to the enhanced well mixed region on the top of the sill (Fig. 3b) compared to previously (Fig. 2b). Similarly at depth in the region of the separation point (z = -40 m) there is increased mixing at t = 16/8T (the end of the second cycle) compared to previously (namely t = T the end of the first cycle) (compare temperature contours in Figs. 2b and 3b). In order to quantify the mixing over the first three tidal cycles the parameter $DN = \overline{N}^2 - N_o^2$ was computed, with N_o the initial buoyancy frequency and $\overline{N}^2$

its average value over a tidal cycle centred at t = 2.5T. By averaging over a tidal cycle, changes in density due to tidal advection were removed. Contours of DN (Fig. 3c) clearly show that significant mixing has occurred during the first three tidal cycles. This leads to a decrease in the temperature gradient in the upper part of the water column, centred at about z = -40 m. A slight increase in temperature gradient centred at about z = -70 m is apparent. These changes in temperature gradient are indicative of mid-water mixing, occurring at about z = -40 m.

This comparison over three tidal cycles illustrates that mixing in the first two-cycle influences the density distribution at the end of the third. In reality freshwater inflow from the head of the loch will tend to re-stratify the region, although it is doubtful if a truly periodic solution in the baroclinic field can be achieved.

3.2 Influence of small-scale (rough/ripple) topography (Calc 2)

In the previous calculation smoothly varying topography was assumed. In reality small-scale undulations in topography will occur both along slopes and the sill crest. Such small scale variations in topography have been observed on a range of sills, banks and shelf slopes (e.g. Inall et al. 2004, 2005, Moum et al. (2007), Klymak and Gregg 2001, Nash and Moum (2001), New and Pingree (1990)). To examine to what extent these influence lee wave generation and subsequent mixing a calculation was performed with the same topography but with the addition of small-scale features along the right hand sill slope (Calc 2, Table 1). By including small-scale topography along just one slope, the extent to which it influences the solution on the sill top and along the other slope can be determined. In essence, “local” and “far field” effects can be separated. In reality a range of small scale topographic features exist in sill regions. Here a typical length scale of 100 m and height of 5 m (Fig. 4a) was chosen to illustrate the effect of small scale topography. Although XD06a, very briefly showed that small scale topography influenced lee waves near the Loch Etive

sill, that was presented in terms of a "snapshot" of lee wave activity and no significant discussion was given. In the present calculation that work is extended to examine the time variability of the flow due to the presence of "small scale ripples", and how the tidally averaged mixing is influenced by the presence of these "ripples". In addition discussion of the importance of the influence of ripple topography upon measured diffusivities and those used in larger scale models has been added.

Comparison of a "snap shot" of temperature, u- and w-components of velocity at t = 2/8T (Fig. 4a) with previous results (Fig. 2a) shows that the main effect of the small scale "ripple" topography upon the temperature and u-velocity fields is confined to the near bed region on the right side of the sill. However, in terms of lee wave generation and hence the vertical component of velocity on the lee side of the sill there is an appreciable difference. Previously (Fig. 2a) at t = 2/8T, lee waves were primarily confined to the slope region extending to x = 1000 m (Fig. 2a). The effect of the small-scale topography is to increase this region to x = 1500 m (Fig. 4a). Similarly the region of temperature inversions and patches of increased u-surface current that were confined to the area between x = 0 and 1000 m, now extends to 1300 m. Later in time (t = 4/8T) a well mixed region on the right hand side of the sill comparable to that found without ripples has developed. This suggests that the main features of the mixing in the upper part of the water column close to the sill are not particularly sensitive to small scale topography. However, at t = 6/8T as the flow reverses and the well mixed region is advected towards the sill, Calc 2 shows that the weakly stratified region at z = -30 m has a larger horizontal extent than previously (Calc 1). This suggests that the generation of lee waves over a larger section of the sill than previously together with their enhanced downstream transport increases the region over which vertical mixing occurs. On the left side of the sill the density field is not appreciably different to previously, suggesting that small scale topographic effects on one side do not influence the other. This difference in

downstream and near sill mixing due to small-scale topography is apparent in the temperature surfaces at the end of the first cycle (compare Figs. 4b and 2b). In addition the u-velocity jet at t = T computed with small-scale topography was found to be stronger and extend from the sill top out to x = 1500 m, as a continuous flow.

As in the first calculation, at t = 10/8T there are appreciable differences in the solution compared to the same time namely t = 2/8T in the first cycle. However these differences are larger (compare Figs. 5a and 3a) than in the first calculation. Also at this time there are substantial differences in the lee wave distribution, as can be seen in the vertical velocity contours (Fig. 5a compared with 3a). Despite these differences in lee wave distribution, the large scale features of the density field in the region of the sill at the end of the second cycle (Fig. 5b) are comparable to those found previously (Fig. 3b). Comparison of DN distributions (Figs. 3c and 5c) also confirms that away from the sill and the bottom boundary layer the large scale features of the mixing are comparable to those found previously. However, the detailed vertical distribution of the temperature and DN field at points in the vicinity of the sill even away from the near bed region but particularly in the lower half of the water column (Fig. 5c) are different. Consequently conclusion concerning eddy diffusivity parameterizations derived by vertically sampling this temperature field will be different from those derived by sampling the temperature field computed with smooth topography and cannot be simply related to local values of water depth, velocity and initial temperature field but must account for enhanced lee wave activity and resulting mixing produced by small scale features. These calculations suggest that the problem of how to parameterize small scale topography, and the associated lee waves to give accurate diffusivities in models that cannot resolve small scale topographic features, will be very difficult.

4. INFLUENCE OF TOPOGRAPHY (SYMMETRIC SILL)

4.1 Smooth topography (Calc 3)

As discussed previously the advantage of using topography representative of Loch Etive is that limited qualitative comparisons of lee wave generation and flow separation can be made with published observations. In addition how these results are changed by the addition of "small scale ripple" topography can be assessed in a "real world" situation. However, the major disadvantage was the short term nature of the calculations. In order to examine the longer term influence of topography upon mixing and the transfer of energy across the internal wave spectrum, a larger domain with more idealized topography is required. Consequently to examine in more detail the influence of small scale (ripple) topography in particular that on the upper part or lower part of the sill slope, and sill width (large scale topography) upon mixing, the previous calculations were repeated using a symmetric sill.

Although some early results in terms of "snap shots" of the temperature and vertical velocity field were presented in a short paper (XD06b), not attempt was made in that paper to assess how changes in topography influenced the time evolution of the flow, and shear instabilities as shown by the Richardson number (R_i) plots presented here. These problems are considered here, as is the influence of a more extensive range of topography than considered in XD06b. In addition the influence of the initial buoyancy frequency upon the tidally averaged mixing is examined. In essence the work presented here extends and elaborates that given in XD06b. In initial calculations (Calcs 3 to 6 in Table 1) both sides of the sill had the same profile as the right hand side of the Loch Etive sill (Fig. 1). Namely the sill depth h_s = 15 m, half width a_o = 1500 m, with water depth on each side fixed at 100 m. In these calculations a larger domain than previously was used so that the longer term effects of sill mixing could be examined without baroclinic waves being reflected from the boundaries. To this end the open boundary was placed at x = -40km, with the closed boundary at x = 40km. In initial calculations (Table 1) the vertical temperature gradient was as previously,

corresponding to N = 0.01 s^{-1}. A detailed analysis of the flow in the Loch Etive calculations (not presented) showed that the sin (ωt) forcing produced a weak long term residual flow. Although this was not significant in short (2 tidal cycle) calculations to avoid it in the long term calculations with the symmetric sill, the forcing was of the form

$$U = F(t)U_o \cos\omega t.$$

Here the ramping function F(t) was used to increase tidal forcing at the open boundary. In essence F(t) increased exponentially from 0 to 1 over a tidal period, after which it was constant at F(t) = 1.

Considering initially Clac 3 (Table 1), as in the Loch Etive calculation during the first tidal cycle, as the tidal velocity above the sill increases, isotherms on the left hand side of the sill upwell, (as in Fig. 2a) and there is advection over the sill. This upwelling and advection of the temperature field over the sill is evident in the time series at x = 0 (centre of the sill) given in Fig. 6a. On the lee side of the sill, the cross sill flow impinges on a water body at rest, and flows down the lee side of the sill with an associated depression of the isotherms. As the flow reverses at about t = 0.3T (Fig. 6a), this depression of the isotherms is swept back over the sill although the isotherms over the sill remain elevated from their initial position. Following an initial "spin up" period of one tidal cycle, a nearly uniform barotropic tidal cycle is established with rapid fluctuations of the isotherms at x = 0 at times following tidal reverse (see temperature time series in Fig. 6a). These fluctuations are associated with hydraulic transitions which occur at about x = ±400 m (as in Fig. 2a) and are subsequently advected onto the sill as the tide reverses. With the present topography and tidal forcing the M_2 component of the tidal velocity at x = 0, is a maximum at t = **n**T, with **n** an integer. In addition higher harmonics of the tide are generated, leading to an increase in tidal velocity prior to t = **n**T , and decrease just after (Fig. 6a). However, in order to examine the influence of small scale topography upon the flow and temperature distributions we will examine them

at two times namely, at t = 8/8T (namely t = T, the end of the first tidal cycle) (short time scale mixing) and 7T (the end of the seventh tidal cycle) (longer time scale), namely at times close to maximum cross sill velocity. By considering t = 7T, the longer term influence of small scale topography upon the solution can be determined.

Temperature contours at t = T, show (Fig. 7a) the presence of density inversions and enhanced mixing in the region of the sill. These are due to the hydraulic transition that occurs on the lee side of the sill with associated wave breaking and shear instabilities produced by the jet that separates from the sill. As previously (Fig. 2a) in the lower half of the water column the flow is near zero. Close to the sill the u-current amplitude shows regions of surface intensification associated with lee waves that are evident in the vertical velocity field (Fig. 7a). The time series at x = 500 m (Fig. 6b) reveals the generation and propagation of lee waves at this point during times of maximum tidal current. Based on the local water depth h = 60 m with N = 0.01 s^{-1}, $F_r = \pi U/hN \approx 3$ for U of order 0.6 m s^{-1} corresponding to the maximum cross sill velocity. This shows that F_r exceeds 1 as far as ±500 m away from the sill crest, although as water depth increases and tidal velocity decreases F_r falls below unity. Hence the flow changes from super-critical to sub-critical via the hydraulic transition in the region of the sill. However, lee waves and the hydraulic transition give rise to temperature spikes that can be advected beyond the sill region into areas where the flow is sub-critical. Consequently the temperature time series at x = 500 m, where the flow is sub-critical (Fig. 6b) has similar characteristics to that given in Fig. 6a, although the vertical displacement and "bounce back" in the upper layers of the water column are not as strong and occur later in time. This later occurrence suggests the displacement was generated upstream, near the sill break, and advected into the region. In addition there is more high frequency variation in the temperature record at times of flood tide due to the presence of lee waves (see u and w time series in Fig. 6b). These were not present over the

sill crest. At ebb tide, lee waves were absent and isotherms in the surface layer showed little time variation.

The Richardson number plot at t = T, reveals (Fig. 8a) unstable regions ($R_i < 0.25$), on the leeside of the sill where the u velocity "jet" Fig. 7a separates from it. In addition away from the sill there are regions of convective overturning due to wave breaking and the associated temperature inversions in the surface layer shown in Fig. 7a. Also beyond this region, from x = 800 m to 1500 m, there is an area of unstable R_i, ($R_i < 0.25$) at a depth of about z = -30 m associated with the jet shown in Fig. 7a.

On the longer time scale, namely at t = 7T, temperature contours (Fig. 7b) show that there has been appreciable mixing in the sill region and at the depth of the jet (compare temperature contours in Figs. 7a and 7b). The extent of the mixing compared with the initial conditions is quantified in the DN distribution (Fig. 7c). The presence of mid-water mixing outside the sill region leads to a weak vertical temperature gradient between z = -10 to –40 m, although a sharper gradient in the surface layer and below this mid-water region is present. This mid-water mixing is an example of "internal mixing" as defined by Van Haren and Howarth (2004). The weaker vertical density gradient in the sill region reduces N, giving for the same U value an increase in F_r, and hence stronger lee waves than found previously (compare w in Figs. 7a and 7b). In addition the intensity of the current jet increases, compared to previously (see Figs. 7a,b). This increase in current together with the change in vertical stratification gives rise to two unstable regions ($R_i < 0.25$) on either side of the weakly stratified layer centred at about z = -40 m between x = 700 m and 1500 m (Fig. 8b). These two unstable regions led to enhanced mixing in the central region of the water column as time progresses.

Time series of temperature and u velocity (Calc 3, Table 1) over tidal cycles 6 to 8 (namely t = 6T and 8T) at x = 0 (Fig. 6c), exhibit similar features to those found in the first

two tidal cycles (compare Figs. 6a and 6c). In particular there is a rapid vertical displacement of the near surface isotherms very close to the start of flood and ebb tide. In essence the displacement occurs at about 0.05T after the start of flood or ebb tide. However, except for the near bed region, the water column is well mixed below this surface layer. The u velocity exhibits a sinusoidal variation with no indication of lee waves, which were also absent in the vertical velocity time series. The cross sill velocity had a shorter flood than ebb time, indicating the presence of higher harmonics generated at the sill. This is consistent with the observations of Inall et al. (2004, 2005) who reported finding higher harmonics. By using the free surface form of the MIT model, the sea surface elevation over the sill can respond to convergences and divergences in the flow field in regions of changing topography. These convergences/divergences give rise to increases/decreases in sea surface elevation. At x = 500 m, time series (Fig. 6d) show significantly stronger lee waves reflecting the reduced stratification found at mid-depth (see temperature time series) and associated increase in F_r compared to initially (Fig. 6b). This arises because reducing N, diminishes the buoyancy restoring force, thereby allowing for an increase in lee wave amplitude. The effect of changes in buoyancy is considered later in the paper.

This calculation (Calc 3, Table 1) clearly shows that the mixing produced in the vicinity of the symmetric sill is comparable to that found with idealized Loch Etive topography. In addition the calculations reveal that on the longer time scale the internal mixing leads to an appreciable reduction in stratification in the region where flow separation occurs, and downstream of the separation point. In the next series of calculations (namely Calcs 4 to 6, Table 1) the influence of small-scale topography upon this is examined. As previously this topography had a length scale of 100 m and height of order 5m. In essence by adding small scale topography the local tidal excursion parameter R_L taken as the ratio of tidal excursion (of order 10 km) to local small scale topography (of order 100 m) is

significantly increased compared to the "smooth" sill case. As R_L is a measure of the non-linearity of the solution, then some change in local lee wave generation is to be expected.

4.2 Additional of small scale (rippled) topography to the upper part of the sill slope (Calc 4)

The addition of small scale rippled topography (Calc 4, Table 1, see Fig. 9a) as often found on sills or banks (e.g. Klymak and Gregg 2001, Nash and Moum 2001) initially (t = 0 to 0.4 T), has little influence on the temperature or velocity time series at x = 0 (compare Figs. 10a and 6a). However, after about 0.4 T (5 hrs) when the tidal flow has reversed, the temperature signal (Fig. 10a) shows small-scale ripples. Based on a background barotropic tidal velocity of on average 10 cm s^{-1}, by this time the temperature field from the left side of the sill has been advected over the sill and back to x = 0. Consequently any effect of the small-scale topography on either side of the sill will appear in the x = 0 time series. In subsequent cycles, particularly the ebb tide cycle between t = 1.2T and 1.8T there is a significant departure of the isotherms from those found previously (compare Figs. 10a and 6a), suggesting an increase in mixing due to the presence of small scale topography. This increase in mixing on the lee side of the sill is evident in the spatial distribution of upper water column isotherms (compare Figs. 7a and 9a). The enhanced mixing leads to a reduction in N in the sill region, with an associated increase in F_r, based on local sill velocity, water depth and value of N. In addition an enhancement in lee wave amplitude compared to previously occurs, as shown in the vertical velocity contours (Figs. 7a and 9a). Also the near surface current velocity increases, with regions of enhanced u velocity due to the presence of lee waves (Fig. 9a). This increase in lee wave activity is evident in the time series at x = 500 m (Fig. 10b). Compared to previously (Fig. 6b) it is apparent (Fig. 10b), that the lee waves are more energetic (note differences in scales between Figs. 6b and 10b) and have a shorter period, reflecting the enhanced mixing due to the presence of small scale topography. In

addition the reduction in N gives rise to an increase in F_r. This increases in lee wave and current velocity amplitude increases the lateral extent of the surface layer of unstable R_i number (compare Figs. 11 and 8a).

The enhancement of mixing in the sill region produced by the small scale rippled topography, on the longer time scale (t = 7T) gives rise in the sill region to a well mixed upper water column (Fig.9b,c). Away from the sill, enhanced mid-water mixing gives rise to a homogeneous water column, centred at about z = –20 m, approximately the depth at which the u current jet leaves the sill (Fig. 9b). In the surface layer, this mid-water mixing produces a thin stratified near surface layer. It is clearly evident from a comparison of DN distributions (Fig. 7c and 9c) on the long term (t = 8T) that the presence of ripples on the upper part of the slope has substantially increased mixing in the upper half of the water column. However at depth, away from the slope there is no substantial difference in stratification. In addition the effect of the ripples is to increase lee wave intensity and the extent of their downstream distribution (compare Figs. 7b and 9b).

This calculation (Calc 4, Table 1) suggests that small scale topography in the upper part of the sill, where the current separates from the sill, will appreciably enhance vertical mixing. The extent to which topography at depth influences mixing is examined in a subsequent calculation.

4.3 Addition of small scale (rippled) topography to the lower part of the sill slope (Calc 5)

The presence of ripples on the lower sill slope region (Calc 5, Table 1) only had a small effect upon the near surface temperature distribution, compared to the smooth topography solution (Fig. 7a). However, at depth in the region of the topography some small-scale displacements of the isotherms not found previously occurred.

4.4 Influence of small-scale variations in upper sill slope small-scale topography (Calc 6)

To examine to what extent the mixing on the lee side of the sill was influenced by small changes in upper slope topography Calc 4 was repeated using the same sinusoidal distribution of topography, but shifted in space by 180° (Clac 6, Table 1). By this means a small "bump" rather than "dip" (Fig. 9a) appeared on the upper part of the slope.

At t = 7T both calculations 4 and 6 show a well-mixed surface layer on the lee side of the sill, extending to x = 1300 m, where there is a surface front (Fig. 9b). Beyond this there is mid-water mixing below a stratified surface layer. Stratification at depth is comparable in both cases. In addition the u current distributions at t = 7T, are not substantially different.

This and previous calculations clearly show that small-scale topography on the upper part of the slope significantly influences mixing on the lee side of the sill. However the exact distribution of the small scale topography does not have an appreciable influence on the solution.

5. INFLUENCE OF SILL WIDTH

5.1 Constant N (Calc 7)

In the previous series of calculations the symmetric sill's width corresponded to that of Loch Etive. In addition the influence of small-scale rippled topography upon sill mixing was examined. This section considers the extent to which sill width, and hence larger scale topography influences mixing. The model domain, tidal forcing, sill depth and water depth were as previously, although the sill width was reduced from 1500 m to 500 m (Fig. 12a). In an initial calculation (Calc 7, Table 1) with this reduced sill width, N = 0.01 s^{-1}, as in the wider sill calculations. Since the tidal forcing velocity remained as previously, then the tidal excursion remained at 10 km, but the tidal excursion parameter R_L increased by a factor of three. Also the sill slope is increased significantly. Therefore the combination of these two factors increases the non-linearity and an increase of lee waves is to be expected.

Although a narrow sill case, and the influence of stratification upon the internal wave field was briefly considered in XD06b, this was only in terms of a "snap shot" of the temperature and vertical velocity field. Here, that work is extended to examine changes in the internal wave field on both the short and long time scale. In addition time series are presented together with Richardson number distributions in order to examine to what extent sill width and vertical stratification influences the internal wave field and associated mixing.

On the short time scale, namely first tidal cycle, the temperature and velocity time series on the top of the sill (x = 0), (Fig. 13a) are in close agreement with those found for the wide sill (Fig. 6a). However, the smaller lateral extent of the sill means that the sill's slope is enhanced, giving rise to a more rapid temporal and spatial fluctuation of the temperature field, as the flow accelerates over the sill. This is evident in the rapid time variation of the 12° isotherm in Fig. 13a as the tide reverses. Also the smaller extent of the sill width, leads to a more rapid downwelling of the density surfaces, and stronger hydraulic transition on the lee side of the sill. This stronger transition produces the near vertical temperature profile at t = T at x = 900 m on the right hand side of the sill (Fig. 12a). On the sill side of this, namely between x = 0 and 900 m, is a region of intense mid-water mixing produced by convective overturning and associated wave breaking. Additional mixing is produced by shear instability due to the jet that separates from the top of the sill (Fig. 12a). Although the mid-water mixing produces a near homogeneous water column between z = -10 m and –40 m, between x = 500 and 800 m, it leads to a significantly stronger near surface temperature gradient. The intensity of this mixing, the associated lee waves and current jet are enhanced compared to previously (compare Figs. 7a and 12a). The increased intensity and shorter period of the lee waves produced with the narrow sill are evident in the time series at x = 500 m (Fig. 13b) compared to the wider sill (Fig. 6b). The spatial extent of the region of enhanced mixing is clearly evident from the R_i number distribution, with $R_i < 0$ implying

convective instability. A region of unstable R_i number ($R_i < 0.25$) extending from the sill, up to x = 800 m, and from z = -10 m to – 30 m on the lee side of the sill occurs at t = T (Fig. 14a). In this area there is intense vertical mixing, which is appreciably larger than in the wide sill case (compare Figs. 8a and 14a).

The enhanced mixing, increased intensity of the u current jet, and enhanced lee wave distribution on the lee side of the narrow sill, on the longer time scale (t = 7T) compared with the wide sill is evident from a comparison of Figs. 7b and 12b. On this longer time scale it is apparent that the more abrupt transition from super-critical to sub-critical flow across the narrow sill produces an enhanced hydraulic transition compared with the wide sill case. This enhanced transition arises from the larger $\partial h/\partial x$ term, with the corresponding increased non-linearity giving rise to a stronger lee wave signal, and current jet. Associated with the hydraulic transition and current jet is an increase in convective overturning and shear instability giving enhanced internal mixing compared to the wide sill case. The appreciable increase in mixing between the two sill cases (narrow and wide) at t =7T, is evident from a comparison of Figs. 8b and 14b. This increased mixing, reduces N, leading to an increase in F_r and amplitude of lee waves. In this calculation N was constant in the vertical. However, in many loch and fjord systems there is a layer of freshwater at the surface (Inall et al. 2004, 2005), giving in essence a two-layer system. The extent to which this influences mixing in the narrow sill case is examined in the next calculation.

5.2 Vertically varying N.

5.2.1 $N_1 = 0.02\ s^{-1}$, $N_2 = 0.01\ s^{-1}$ (Calc 8)

To examine the influence of adding a strongly stratified surface layer with buoyancy frequency $N_1 = 0.02\ s^{-1}$, and thickness $h_1 = 20$ m the previous calculation was repeated (Calc 8, Table 1) with this additional layer. At depth, the same stratification as previously, namely $N_2 = 0.01\ s^{-1}$ was applied. The effect of increasing the buoyancy in the surface layer which

intersects the top of the sill, is to oppose the displacement of the temperature surfaces on the lee of the sill. In addition the F_r number on the top of the sill is reduced to half that when N = 0.01 s^{-1}. Consequently the hydraulic transition is reduced with an associated reduction in convective overturning and mixing in the upper part of the water column compared to previously (compare Figs. 15a and 12b). In addition the amplitude and lateral extent of the lee waves formed on the downstream side of the sill are reduced compared to those found previously, as shown by the vertical velocity distributions in Figs. 15a and 12b.

However, on the lee side of the sill, a current jet and flow separation still occurs but at z = -40 m (deeper than previously) and about the position of the transition between the two layers (Fig. 15a). Associated with this jet is a downstream region of shear instability with R_i < 0.25 and enhanced mixing (Fig. 15b). The width of this mixing region, and the intensity of the mixing within it, is appreciably smaller than previously (compare Figs. 15b and 14b). This mixing leads to a reduction in temperature gradient near the base of the surface layer in the sill region, but to an increase in temperature gradient in the interface region between top and bottom layers. Vertical velocity contours and time series at various locations did not show any appreciable lee wave signal away from the top of the sill.

This suggests that the N value in the layer which intersects the upper part of the sill controls the magnitude of the hydraulic transition and associated convective mixing. Increasing this value, decreases F_r in the upper water column with an associated decrease in lee waves. However the shear instability due to the jet that separates from the sill remains and enhances mixing at depth, downstream from the sill.

5.2.2 $N_1 = 0.01\ s^{-1}$, $N_2 = 0.005\ s^{-1}$ (Calc9)

Repeating the calculation with $N_1 = 0.01\ s^{-1}$ and $N_2 = 0.005\ s^{-1}$ (Calc 9, Table 1), gives a surface distribution of temperature on the lee side of the sill comparable to that found

with constant N = 0.01 s^{-1} (compare Figs. 12b and 16a). Similarly the u current distribution, shows a jet leaving the upper part of the sill as found previously with N = 0.01 s^{-1}.

This confirms, as found previously, that the buoyancy in the surface layer is the primary factor controlling the downstream hydraulic transition, current jet and hence mixing. This suggests that a local sill Froude number based on sill velocity, water depth and stratification is more critical than one computed with total water depth and mean buoyancy. The reduced value of N at depth does have some effect on the lee wave distribution, the amplitude and downstream propagation of which increases as N_2 is reduced. The reduced buoyancy frequency in the lower part of the water column, together with the enhanced lee wave amplitude, leads on the longer time scale to a reduction in R_i number in the lower half of the water column compare to N = 0.01 s^{-1}. However, the Richardson number distribution in the upper part of the water column (compare Figs. 14b and 16b) is comparable to that found with N = 0.01 s^{-1}.

6. CONCLUDING REMARKS

A non-hydrostatic model of tidal flow over idealized topography representing the sill at the entrance to a loch or fjord has been used to investigate the influence of small scale rippled topography upon internal waves in the sill region. In addition the effect of sill width and hence sill slope upon the generation of the internal tide and its higher harmonics was also examined. In a final series of calculations the extent to which the profile of buoyancy influences the mixing was considered.

Initially tidal flow over idealized smooth topography representing the sill at the entrance to Loch Etive was used. Short time scale calculations (of the order of two tidal cycles) showed that the model could reproduce the major observed (Inall et al. 2004, 2005) features of the flow, internal lee wave generation and mixing in the region. Hence, although idealized topography and a cross section model were used, it could account for the major

observed processes in sill regions. In a subsequent series of calculations, small scale topographic "ripples" were added to the steeper side of the sill, where observations had been made (Inall et al. 2004, 2005). This had the effect of appreciably influencing mixing on the lee side of the sill. Since this mixing occurs at the level of the thermocline, in essence "internal mixing" (Van Haren and Howarth 2004) rather than "external mixing" as in wind forced surface turbulence it has an appreciable influence upon across thermocline exchange.

The main problem with these initial calculations was that the model domain was small, since it had been chosen to represent Loch Etive. To enable a more detailed analysis of longer term mixing and energy distribution to be performed the model domain was extended. In addition a symmetric sill was used so that the influence of sill width could be considered. Calculations using a wide sill, initially without and subsequently with various small scale topographic ripples, showed that small scale topography on the upper slope of the sill enhanced the long term mixing. Small scale topography on the lower half of the slope had a marginal effect upon the mixing. As the sill width was reduced, mixing below the surface layer significantly increased above that found with the wide sill. These calculations showed that not only did sill width control the mixing, but small scale ripples on a wide sill appreciably enhanced the local mixing.

Subsequent calculations with the narrow sill and vertical stratification representing a two layer situation (e.g. a fresh surface layer above a stratified bottom layer), showed that upper layer buoyancy had a major effect upon the intensity of the hydraulic transition. In addition it influenced the magnitude of lee waves. This reduction in hydraulic transition intensity and lee wave magnitude as N increased in the surface layer led to a decrease in mixing in the lee of the sill.

These calculations which are summarised in Table 1 clearly show that sill width as demonstrated from the comparison of Calcs 3 and 7 (Table 1), on both the short and long

time scale, influences mixing on the lee side of the sill. This arises because as sill width is decreased then for a given across sill velocity U_s, the ratio of tidal excursion to topographic length scale increases. As shown this leads to an increase in the non-linear nature of the problem with a corresponding increase in mixing. For a given sill half width (Calc 3), the addition of rippled topography to the upper part of the sill (Calc 4) clearly influences midwater mixing on the lee side of the sill. This is because small scale topography in this region, where flow separation occurs and lee waves are generated, influences the lateral extent of the region of unstable R_i number. This change in the area of unstable R_i number leads to enhanced vertical mixing. For the case in which the small scale topography is added to the lower part of the sill (Calc 5, Table 1), because this is well removed from the area of current separation or lee wave generation it has no significant influence upon the mixing. In addition from a detailed comparison of Calcs 4 and 6, the exact form of the topography on the upper part of the sill does not appreciable influence mixing. Additional calculations with a smooth narrow sill (Calcs 7 to 9, Table 1) clearly show that stratification in the upper layer has a greater influence upon mixing than that at depth.

This series of calculations clearly shows that if a model has a coarse grig in the region of a narrow sill such as that used here in calculations 7 to 9, then the ratio of tidal excursion to topographic length scale will be artificially reduced resulting in a decrease in vertical mixing. This suggests that to compensate for this it will be necessary to enhance vertical mixing in such models on the lee side of sills.

Even when the grid is sufficiently fine to resolve the sill, calculations 3 to 6, suggest that if such a grid cannot resolve small scale topography on the sill sides, particularly that on the upper part of the sill slope, then again vertical mixing will have to be enhanced in the sill region. Besides having implications for the development of numerical models, these results have some implications for the design of experimental programmes. In particular they

suggest that besides precise current and mixing measurements of the form made by Inall et al. (2004, 2005) on the lee side of Loch Etive, detailed measurements of small scale topography and stratification in the upper part of the sill and the adjacent water column are required for rigorous model validation. In essence, existing data sets are not sufficiently comprehensive to allow for a rigorous skill assessment of simulation models to be performed. To permit such quantitative comparisons more comprehensive data sets need to be collected, which will contain details of the small scale variations in bottom topography.

Acknowledgements

The authors are indebted to the reviewers for their constructive comments and L Parry and E. Ashton for typing the text.

REFERENCES

Afanasyev, Y.D. and W.R. Peltier (2001) On breaking internal waves over the sill in Knight Inlet. Proceedings of the Royal Society London, A457, 2799-2825.

Baines, P.G. (1995) Topographic effects on stratified flows. Cambridge Monographs on Mechanics. Cambridge University Press.

Berntsen, J. and G.K. Furnes (2005) Internal pressure errors in sigma-coordinate ocean models – sensitivity of the growth of the flow to the time stepping method and possible non-hydrostatic effects. Continental Shelf Research, 25, 829-848.

Berntsen J., Xing J. and Davies, A.M. (2008) Numerical studies of internal waves at a sill: sensitivity to horizontal grid size and sub-grid scale mixing. Continental Shelf Research, 28, 1376-1393.

Berntsen, J., Xing, J., Davies, A.M.(2009) Numerical studies of flow over a sill : sensitivity to the non-hydrostatic effects to grid size. Ocean Dynamics, DOI 10.1007/s10236-009-0277-0.

Cummins P. (2000) Stratified flow over topography : time-dependent comparisons between model solutions and observations. Dyn. Atmos. Ocean 33, 43-72.

Davies, A.M. and Xing, J. (2007) On the influence of stratification and tidal forcing upon mixing in sill regions. Ocean Dynamics 57, 431-452.

Dewey, R. Richmond, D. and Garrett, C. (2005) Stratified tidal flow over a bump. Journal of Physical Oceanography, 35, 1911-1927.

Farmer, D.M. and Armi, L. (2001) Stratified flow over topography : model versus observations. Proceedings of the Royal Society of London A, A457, 2827-2830.

Gerkema, T. (2002) Application of an internal tide generation model to baroclinic spring-neap cycles. Journal of Geophysical Research, 107(C9), 3124, doi:10.1029/2001JC001177.

Heggelund, Y., F. Vikebø, J. Berntsen and G. Furnes (2004) Hydrostatic and non-hydrostatic studies of gravitational adjustment over a slope. Continental Shelf Research, 24, 2133-2148.

Inall, M.E., F.R. Cottier, C. Griffiths and T.P. Rippeth (2004) Sill dynamics and energy transformation in a jet fjord. Ocean Dynamics, 54, 307-314.

Inall, M.E., T.P. Rippeth, C. Griffiths and P. Wiles (2005) Evolution and distribution of TKE production and dissipation within stratified flow over topography. Geophys. Res. Lett., 32, L08607, doi:10.1029/2004GL022289.

Jeans, D.R.G. and T.J. Sherwin (2001) The evolution and energetics of large amplitude non-linear internal waves on the Portuguese shelf. Journal of Marine Research, 59, 327-353.

Klymak, J.M. and M.C. Gregg (2001) Three-dimensional nature of flow near a sill. Journal of Geophysical Research, 106, 22,295-22,311.

Lamb, K.G. (1994) Numerical experiments of internal wave generation by strong tidal flow across a finite amplitude bank edge. Journal of Geophysical Research, 99, 843-864.

Legg, S. and A. Adcroft (2003) Internal wave breaking at concave and convex continental slopes. Journal of Physical Oceanography, 33, 2224-2246.

Legg, S. and Huijts K.M.H. (2006) Preliminary simulations of internal waves and mixing generated by finite amplitude tidal flow over isolated topography. Deep Sea Research 53, 140-156.

Marshall, J., C. Hill, L. Perelman and A. Adcroft (1997a) Hydrostatic, quasi-hydrostatic and nonhydrostatic ocean modelling. J. Geophys. Res., 102, 5733-5752.

Marshall, J., A. Adcroft, C. Hill, L. Perelman and C. Heisey (1997b) A finite-volume incompressible Navier Stokes model for studies of the ocean on parallel computers. Journal Geophysical Research, 102, 5753-5766.

Mellor, G.L. and T. Yamada (1982) Development of a turbulence closure model for geophysical fluid problems. Reviews in Geophysics and Space Physics, 20, 851-875.

Moum, J.N., J.M. Klymak, J.D. Nash, A. Perlin and W.D. Smyth (2007) Energy transport by non-linear internal waves. Journal of Physical Oceanography, 37, 1968-1988.

Nakamura, T., T. Awaji, T. Hatayama and K. Akitomo (2000) The generation of large-amplitude unsteady lee waves by sub-inertial K_1 tidal flow: a possible vertical mixing mechanism in the Kuril Straits. Journal of Physical oceanography, 30, 1601-1621.

Nakamura, T. and T. Awaji (2001) A growth mechanism for topographic internal waves generated by an oscillatory flow. Journal of Physical Oceanography, 31, 2511-2524.

Nash, J.D. and J.N. Moum (2001) Internal hydraulic flows on the continental shelf: High drag states over a small bank. Journal of Geophysical Research, 106, 4593-4611.

New, A.L. and R.D. Pingree (1990) Evidence for internal tidal mixing near the shelf break in the Bay of Biscay. Deep-Sea Research, 37, 1783-1803.

Rippeth, T.P., M.R. Palmer, J.H. Simpson, N.R. Fisher and J. Sharples (2005) Thermocline mixing in summer stratified continental shelf seas. Geophyscal Research Letters, 32 L05602, doi:10.1029/2004GL022104.

Saenko, O.A. and W.J. Merrifield (2005) On the effect of topographically enhanced mixing on the global ocean circulation. Journal of Physical Oceanography, 35, 826-834.

Saenko, O.A. (2006) The effect of localised mixing on the ocean circulation and time-dependent climate change. Journal of Physical Oceanography, 36, 140-160.

Scotti, A., Beardsley, R.C., Butman, B.(2007) Generation and propagation of nonlinear internal waves in Massachusetts Bay. Journal of Geophysical Research, 112, C10001, doi:10.1029/2007JC004313.

Scotti, A. and Mitran, S.(2008) An approximated method for the solution of elliptic problems in thin domains : application to non-linear internal waves. Ocean modelling 25, 144-153.

Spall, M.A. (2001) Large scale circulations forced by localized mixing over a sloping bottom. Journal of Physical Oceanography, 31, 2369-2384.

Stashchuk, N., Inall, M., and Vlasenko, V. (2007) Analysis of supercritical stratified tidal flow in a Scottish fjord. Journal of Physical Oceanography, 37, 1793-1810.

Stigebrandt, A. and J. Aure (1989) Vertical mixing in basin waters of fjords. Journal of Physical Oceanography, 19, 917-926.

Stigebrandt, A. (1999) Resistance to barotropic tidal flow in straits by baroclinic wave drag. Journal of Physical Oceanography, 29, 191-197.

Van Haren, H. and J. Howarth (2004) Enhanced stability during reduction of stratification in the North Sea. Continental Shelf Research, 24, 805-819.

Van Haren, H. (2006) Non-linear motions at the internal tide source. Geophysics Research Letters, 33, L11605, doi:10.1029/2006GL025851.

Vlasenko, V., Stashchuk, N. and Hutter, K. (2002) Water exchange in fjords induced by tidally generated internal lee waves. Dynamics of Atmospheres and Oceans, 35, 63-89.

Vlasenko, V., Stashchuk, N. and Hutter, K. (2005) Baroclinic tides: Theoretical modeling and observational evidence. Cambridge University Press.

Xing, J. and A.M. Davies (1998) A three-dimensional model of internal tides on the Malin-Hebrides shelf and shelf edge. Journal of Geophysical Research, 103, 27821-27847.

Xing, J. and A.M. Davies (1999) The influence of topographic features and density variations upon the internal tides in shelf edge regions. International Journal for Numerical Methods in Fluids, 31, 535-577.

Xing, J. and A.M. Davies (2005) Influence of a cold water bottom dome on internal wave trapping. Geophysical Research Letters, 32, L03601, doi:10.1029/2004GL021833.

Xing, J. and A.M. Davies (2006a) Processes influencing tidal mixing in the region of sills. Geophysical Research Letters, 33, L04603,doi:10.1029/2005GL025226.

Xing, J. and A.M. Davies (2006b) Influence of stratification and topography upon internal wave spectra in the region of sills. Geophysical Research Letters, 33, L23606, doi:10.1029/2006GL028092.

Xing, J. and A.M. Davies (2007) On the importance of non-hydrostatic processes in determining tidal induced mixing in sill regions. Continental Shelf Research, 27, 2162-2185.

Zhai, X., R.J. Greatbatch and J. Zhao (2005) Enhanced vertical propagation of storm-induced near-inertial energy in an eddying ocean channel model. Geophysical Research Letters. 32:L18602 DOI 10.10291/2005GLO23643.

Table 1: Summary of parameters used in the calculations

Calc.	Sill Half Width a_o(m)	Small Scale Rippled Topography	Sill Form	Buoyancy Frequency N (s^{-1})
1	1500	No	Loch Etive	0.01
2	1500	Yes	Loch Etive	0.01
3	1500	No	Symmetric	0.01
4	1500	Yes (Upper)	Symmetric	0.01
5	1500	Yes (Lower)	Symmetric	0.01
6	1500	Yes (Upper + 180°)	Symmetric	0.01
7	500	No	Symmetric	0.01
8	500	No	Symmetric	0.02/0.01
9	500	No	Symmetric	0.01/0.005

Note: For N two values e.g. 0.02/0.01 under buoyancy frequency refers to vertically varying stratification with $N_1 = 0.02\ s^{-1}$, $N_2 = 0.01\ s^{-1}$.

FIGURE CAPTIONS

Fig. 1: Region covered by the Loch Etive model, with initial temperature distribution T(°C) (contour interval, c.i. = 0.5°C) and position of sill at x = 0, tidal open boundary forcing (x = - 6500 m), and closed boundary (x = 15,000 m).

Fig. 2a: Subdomain of the region showing temperature field (°C, c.i. = 0.5), u and w velocity (cm s^{-1}), (see colour scale for magnitude) at t = 2/8T, where T is tidal period.

Fig. 2b: As Fig. 2a, but at t = T, and not w.

Fig. 3a: As Fig. 2a, but at t = 10/8T.

Fig. 3b: As Fig. 3a, but at t = 2T, and not w.

Fig. 3c: Contours of DN (see colour scale for magnitude) the change in the square of buoyancy frequency over the first three tidal cycles.

Fig. 4a: As Fig. 2a, at t = 2/8T, with the addition of small scale topography.

Fig. 4b: As Fig. 4a, but at t = T, and not w.

Fig. 5a: As Fig. 4a, but for the second tidal cycle, namely at t = 10/8T.

Fig. 5b: As Fig. 4a, but for the second tidal cycle, namely at t = 2T, and not w.

Fig. 5c: Contours of DN (see colour scale for magnitude) the change in the square of buoyancy frequency between initial conditions and those at t = 3T.

Fig. 6: Time series of temperature, u and w velocity (see colour scale for magnitude) in the region of the symmetric sill for:

(a) First two tidal cycles at x = 0 m, but not w

(b) First two tidal cycles at x = 500 m

(c) Cycles 6 to 8 at x = 0 m, but not w

(d) Cycles 6 to 8 at x = 500 m

Fig. 7: Sub-domain of the region covering the symmetric sill at x = 0, showing the temperature field (°C, c.i. = 0.5), u and w velocity (see colour scale for magnitude) at (a) t = T, (b) t = 7T where T is the tidal period

Fig. 7c: Contours of DN (see colour scale for magnitude), the change in the square of buoyancy frequency between the initial conditions and those at t = 8T.

Fig. 8: Contours of Richardson number R_i and temperature (°C) (c.i. = 0.5°C) at (a) t = T, (b) t = 7T.

Fig. 9: Sub-domain of the region covering the symmetric sill with upper slope ripples showing the temperature field (°C, c.i. = 0.5), u and w velocity (see colour scale for magnitude) at (a) t = T and (b) t = 7T.

Fig. 9c: Contours of DN (see colour scale for magnitude), the change in buoyancy frequency between the initial conditions and those at t = 8T, in the case of "small scale ripple topography".

Fig. 10: Time series of temperature T, u and w velocity over the first two tidal cycles for the symmetric sill with upper slope ripples, at (a) x = 0 m, but not w and (b) x = 500 m.

Fig. 11: Contours of Richardson number (R_i) and temperature (°C) (c.i. = 0.5°C) for the symmetric sill case with upper slope ripples at t = T.

Fig. 12: Sub-domain of the region covering the narrow symmetric sill showing the temperature field (°C, c.i. = 0.5), u and w velocity at (a) t = T, and (b) t = 7T.

Fig. 13: Time series of temperature T, u and w velocity over the first two tidal cycles, for the narrow symmetric sill at (a) x = 0, but no w, and (b) x = 500 m with w included.

Fig. 14: Contours of Richardson number (R_i) and temperature (°C) (c.i. =0.5°C) for the narrow sill case for (a) t =T, (b) t = 7T.

Fig. 15a: As Fig. 12, but for vertically varying N with upper layer buoyancy frequency N_1 = 0.02 s^{-1}, and lower layer N_2 = 0.01 s^{-1} at t = 7T.

Fig. 15b: Contours of Richardson number (R_i) and temperature (°C) (c.i. = 0.5°C) for the narrow sill case with vertically varying N, namely $N_1 = 0.02\ s^{-1}$, $N_2 = 0.01\ s^{-1}$ at t = 7T.

Fig. 16a: As Fig. 15a, but for $N_1 = 0.01\ s^{-1}$ and $N_2 = 0.005\ s^{-1}$ at t = 7T.

Fig. 16b: As Fig. 15b, but for $N_1 = 0.01\ s^{-1}$ and $N_2 = 0.005\ s^{-1}$ at t = 7T.

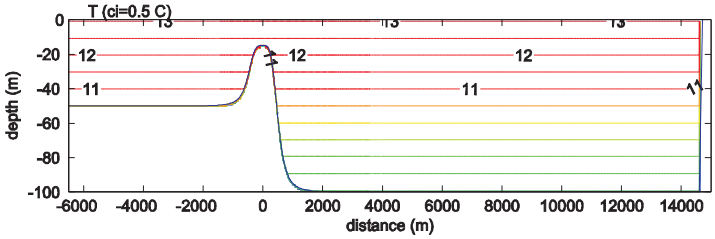

1

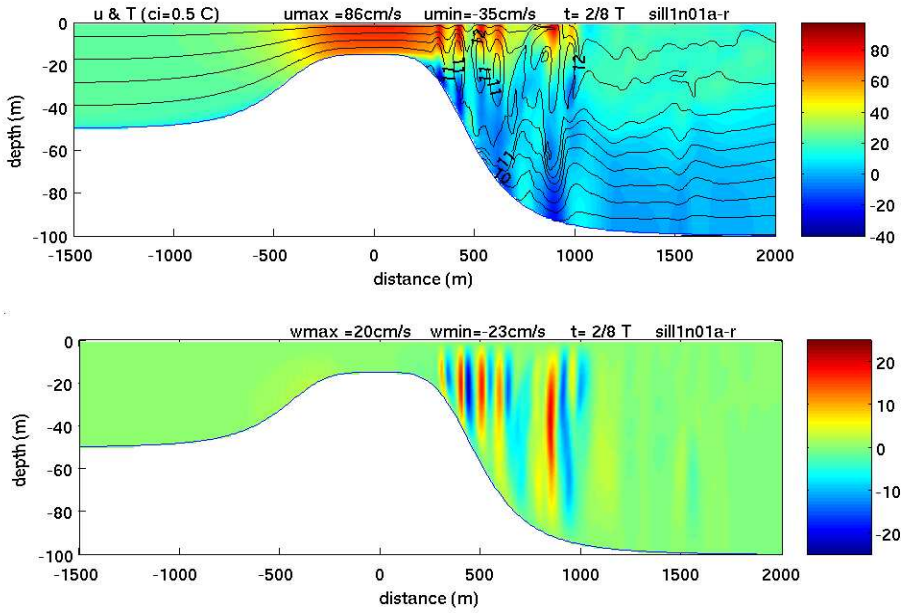
u & T (ci=0.5 C)
umax =86cm/s
umin=-35cm/s
t= 2/8 T
sill1n01a-r
depth (m)
distance (m)
wmax =20cm/s
wmin=-23cm/s
t= 2/8 T
sill1n01a-r
depth (m)
distance (m)

2a

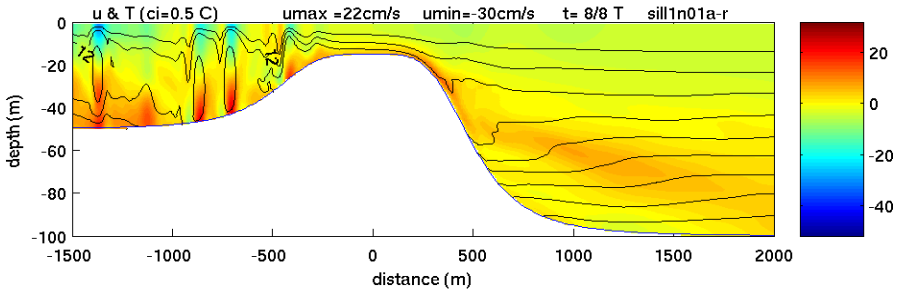
u & T (ci=0.5 C)
umax =22cm/s
umin=-30cm/s
t= 8/8 T
sill1n01a-r
depth (m)
distance (m)

2b

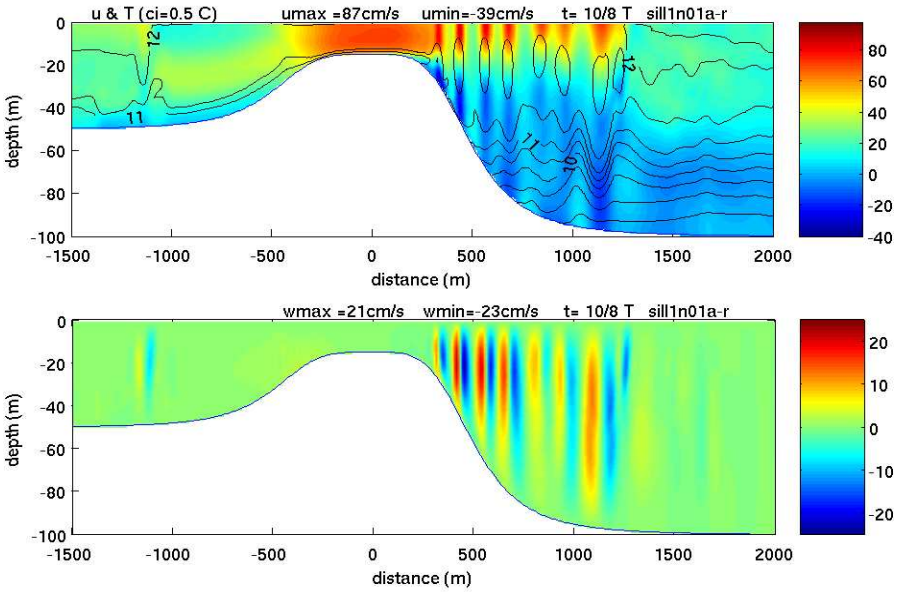
u & T (ci=0.5 C)
umax =87cm/s
umin=-39cm/s
t= 10/8 T
sill1n01a-r
depth (m)
distance (m)
wmax =21cm/s
wmin=-23cm/s
t= 10/8 T
sill1n01a-r
depth (m)
distance (m)

3a

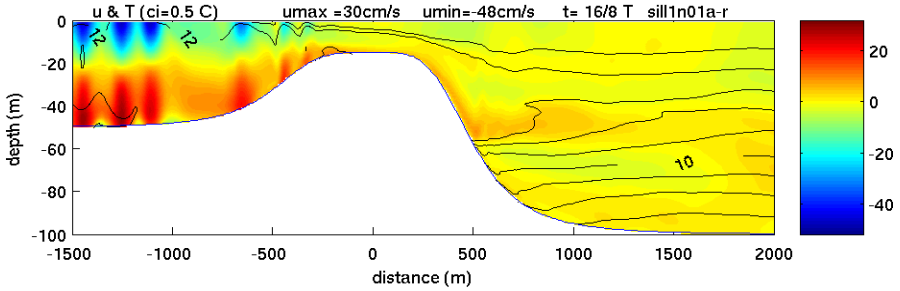
u & T (ci=0.5 C)
umax =30cm/s
umin=-48cm/s
t= 16/8 T
sill1n01a-r
depth (m)
distance (m)

3b

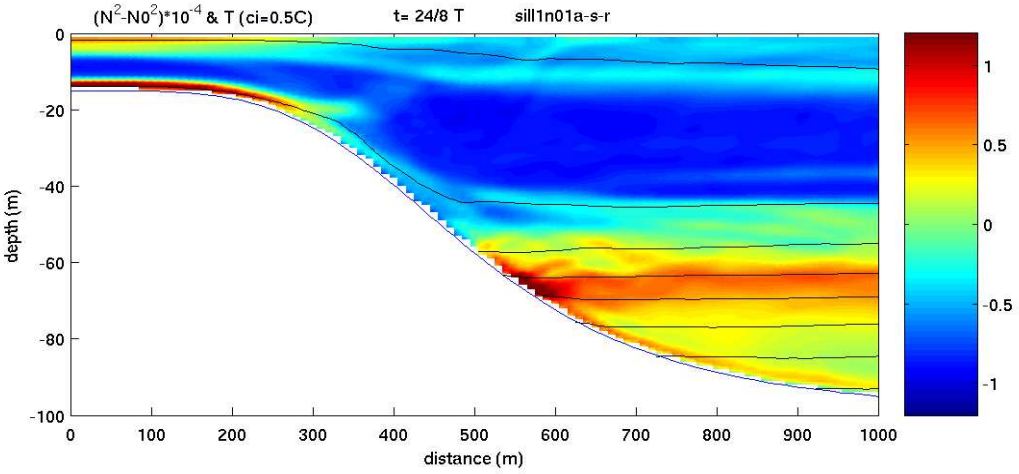
(N2-N02)*10-4 & T (ci=0.5C)
t= 24/8 T
sill1n01a-s-r
depth (m)
distance (m)

3c

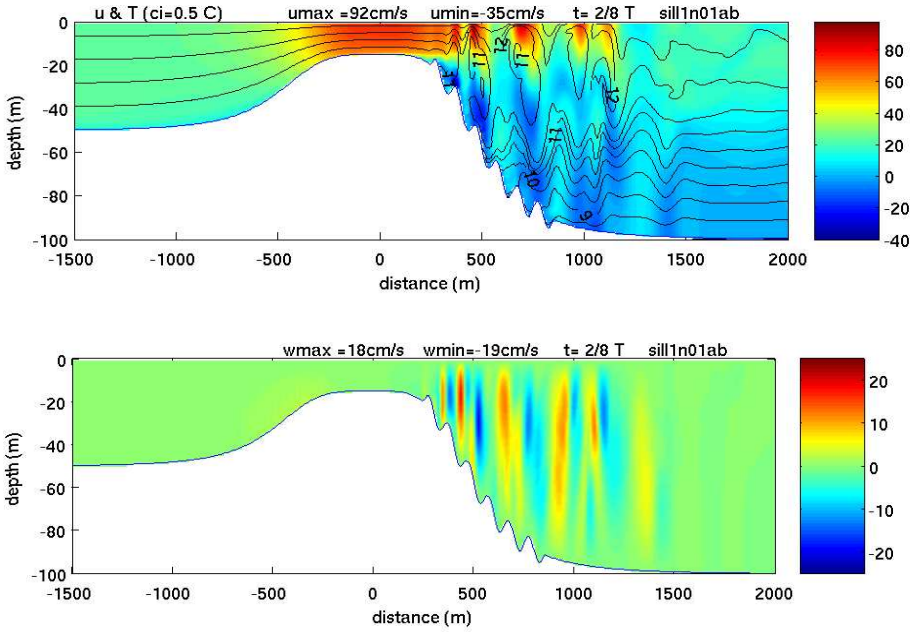
u & T (ci=0.5 C)
umax =92cm/s
umin=-35cm/s
t= 2/8 T
sill1n01ab
depth (m)
distance (m)
wmax =18cm/s
wmin=-19cm/s
t= 2/8 T
sill1n01ab
depth (m)
distance (m)

4a

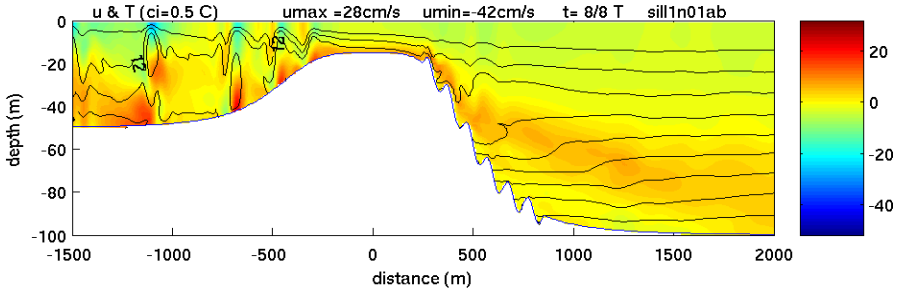
u & T (ci=0.5 C)
umax =28cm/s
umin=-42cm/s
t= 8/8 T
sill1n01ab
depth (m)
distance (m)

4b

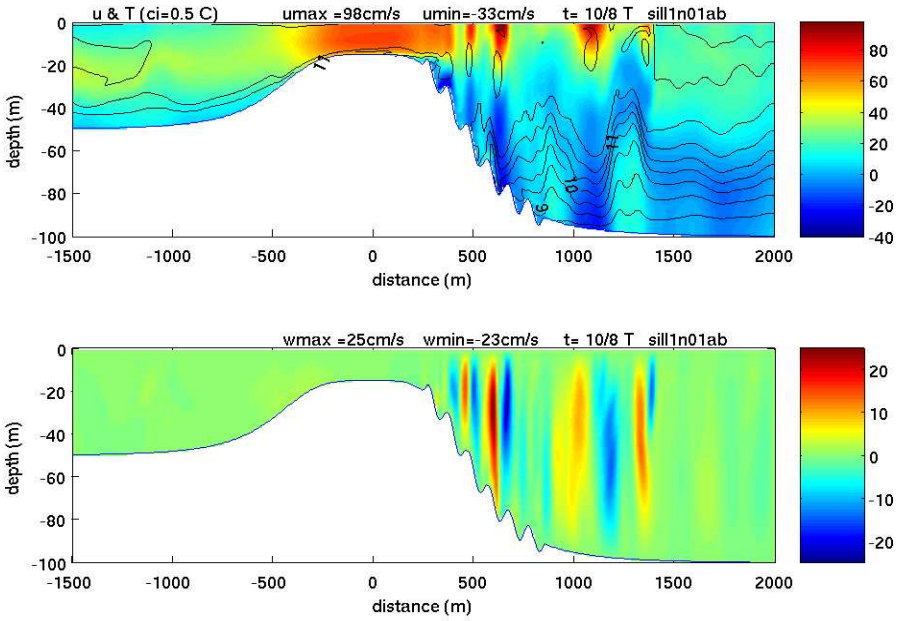
u & T (ci=0.5 C)
umax =98cm/s
umin=-33cm/s
t= 10/8 T
sill1n01ab
depth (m)
distance (m)
wmax =25cm/s
wmin=-23cm/s
t= 10/8 T
sill1n01ab
depth (m)
distance (m)

5a

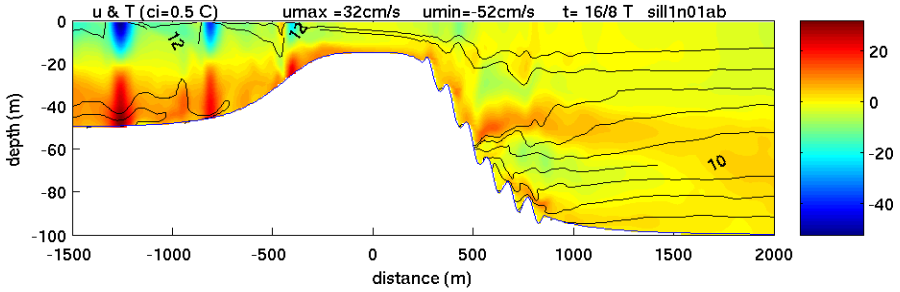
u & T (ci=0.5 C)
umax =32cm/s
umin=-52cm/s
t= 16/8 T
sill1n01ab
depth (m)
distance (m)

5b

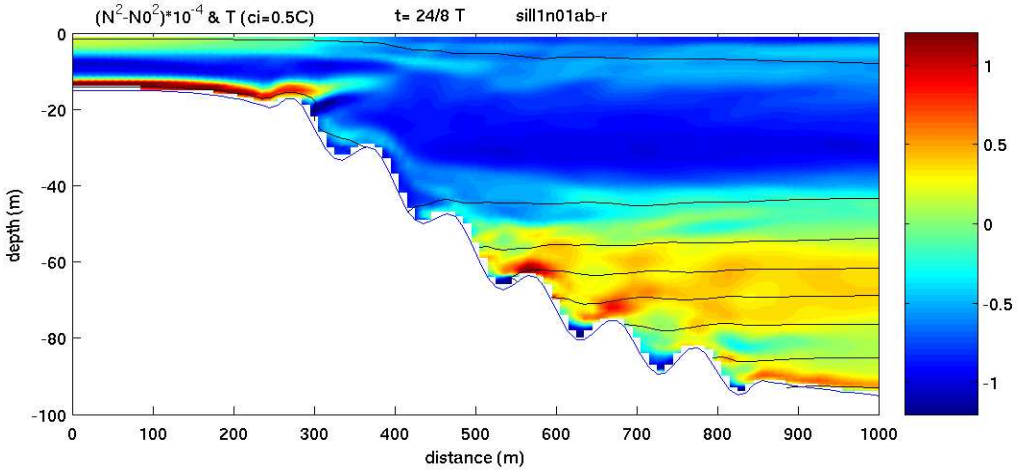
(N2-N02)*10-4 & T (ci=0.5C)
t= 24/8 T
sill1n01ab-r
depth (m)
distance (m)

5c

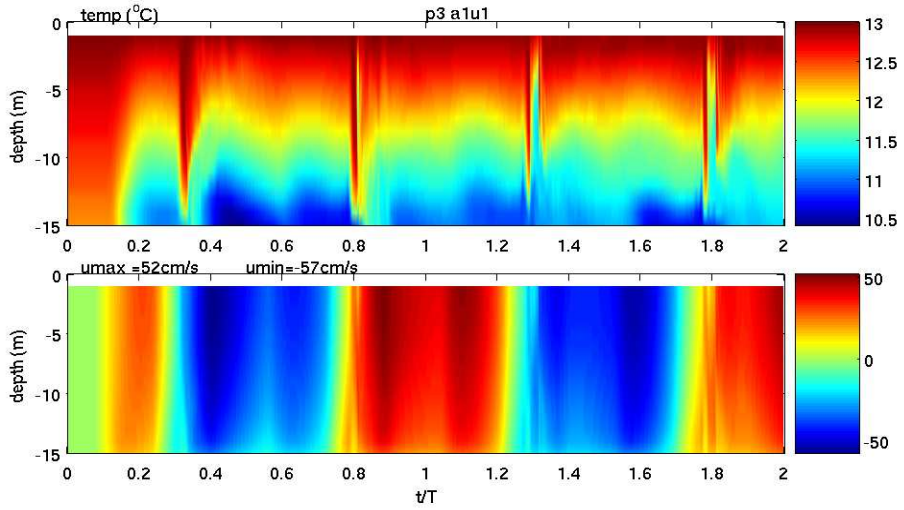
temp (°C)
p3 a1u1
depth (m)
umax =52cm/s
umin=-57cm/s
t/T

6a

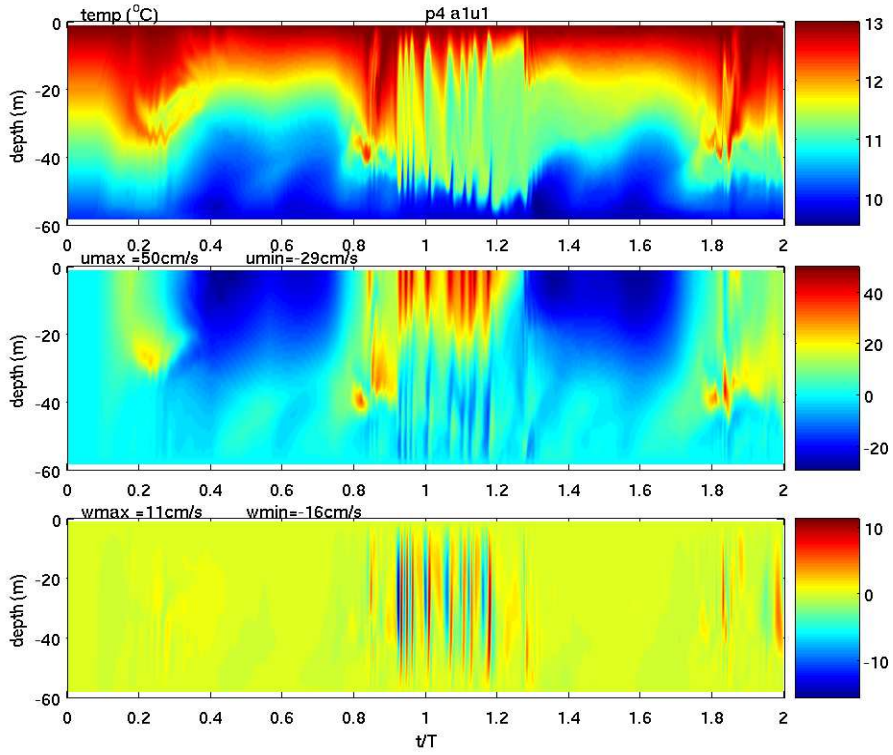
temp (°C)
p4 a1u1
depth (m)
umax =50cm/s
umin=-29cm/s
wmax =11cm/s
wmin=-16cm/s
t/T

6b

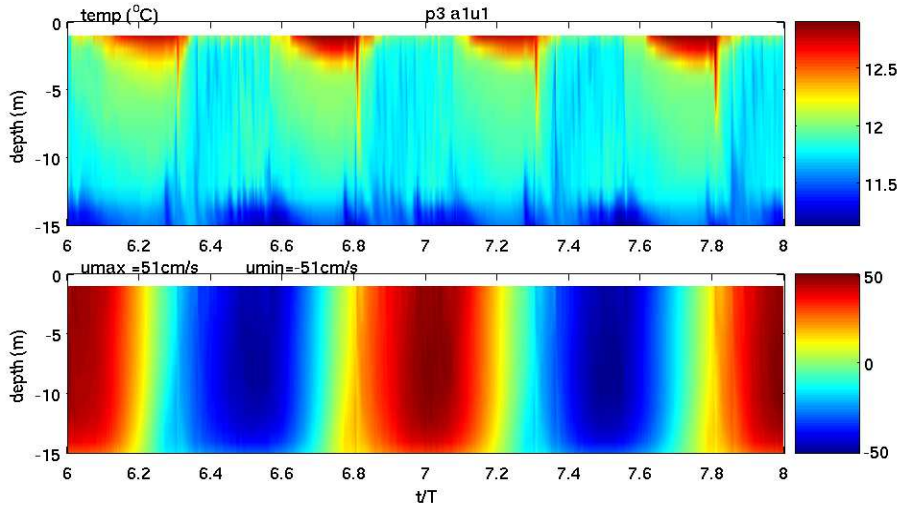
temp (°C)
p3 a1u1
depth (m)
umax =51cm/s
umin=-51cm/s
t/T

6c

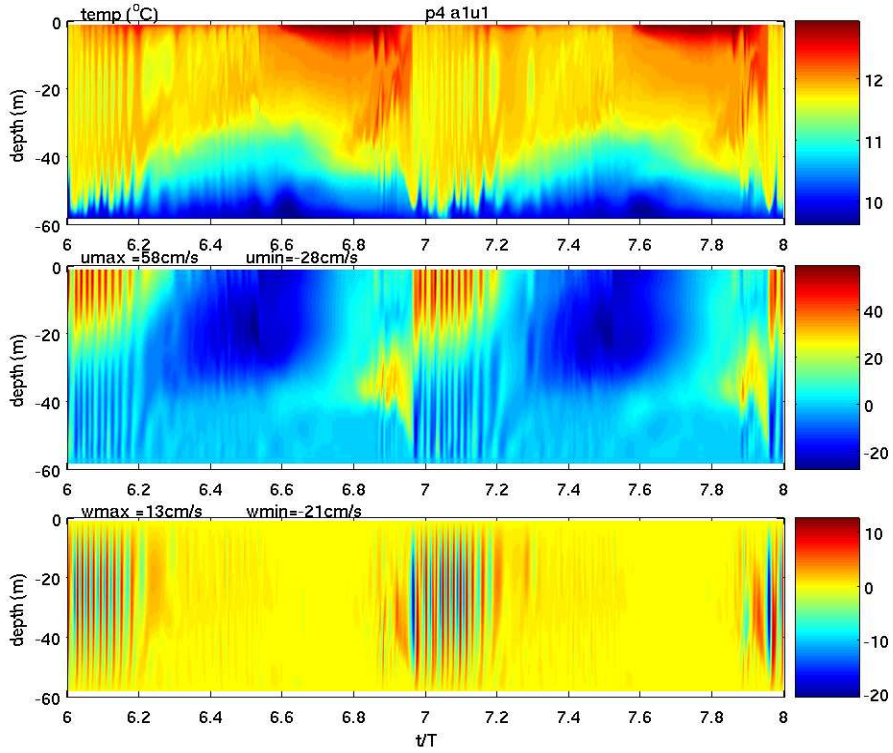
temp (°C)
p4 a1u1
depth (m)
umax =58cm/s
umin=-28cm/s
wmax =13cm/s
wmin=-21cm/s
t/T

6d

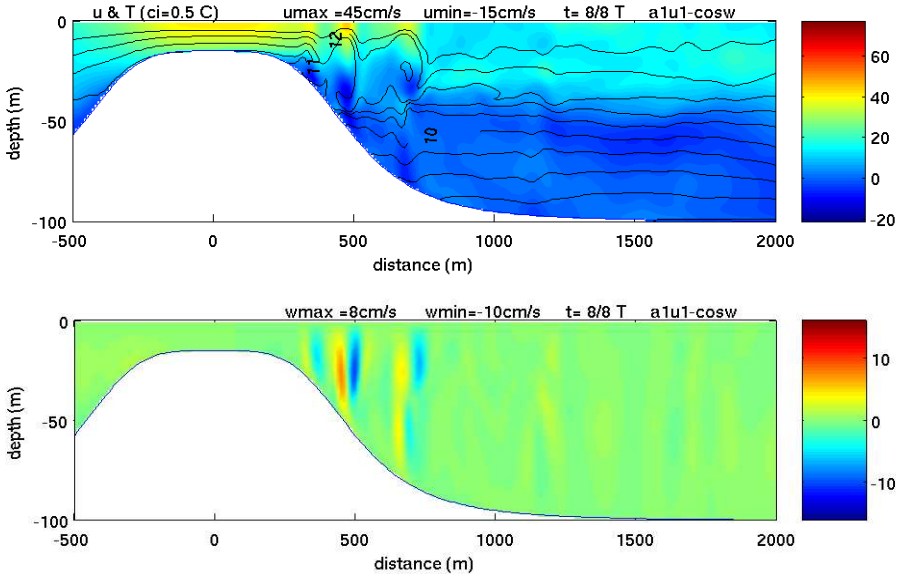
u & T (ci=0.5 C) umax =45cm/s umin=-15cm/s t= 8/8 T a1u1-cosw
depth (m)
distance (m)
wmax =8cm/s wmin=-10cm/s t= 8/8 T a1u1-cosw
depth (m)
distance (m)

7a

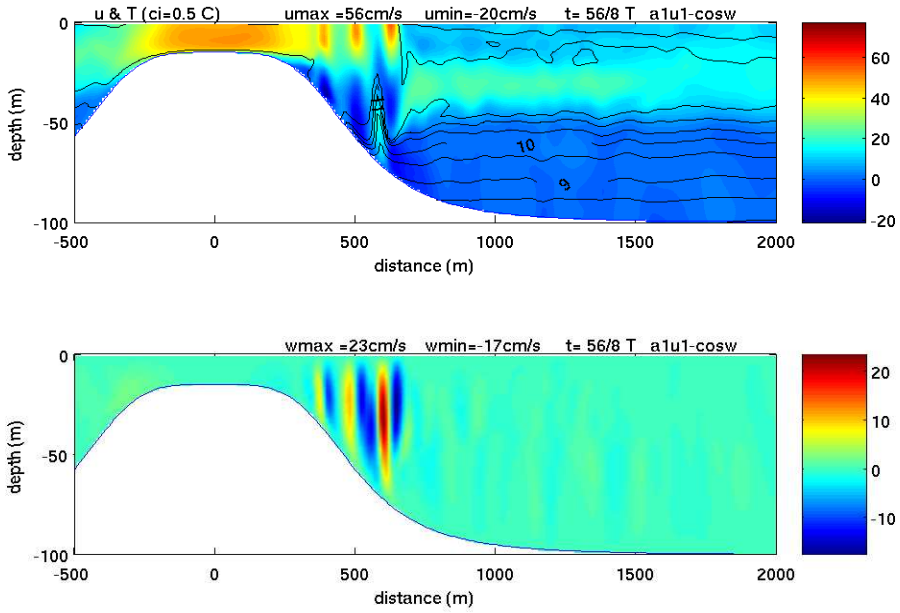
u & T (ci=0.5 C) umax =56cm/s umin=-20cm/s t= 56/8 T a1u1-cosw
depth (m)
distance (m)
wmax =23cm/s wmin=-17cm/s t= 56/8 T a1u1-cosw
depth (m)
distance (m)

7b

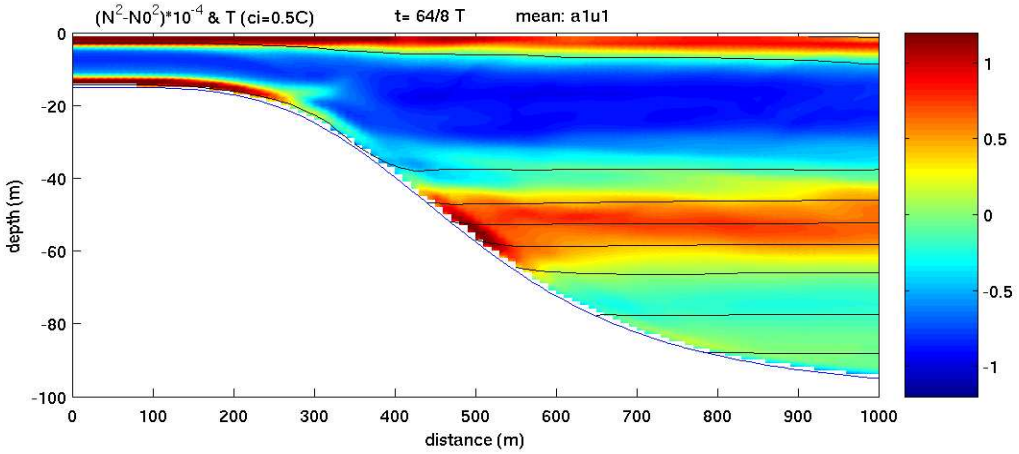
(N2-N02)*10-4 & T (ci=0.5C)
t= 64/8 T
mean: a1u1
depth (m)
distance (m)
0
-20
-40
-60
-80
-100
0
100
200
300
400
500
600
700
800
900
1000
1
0.5
0
-0.5
-1

7c

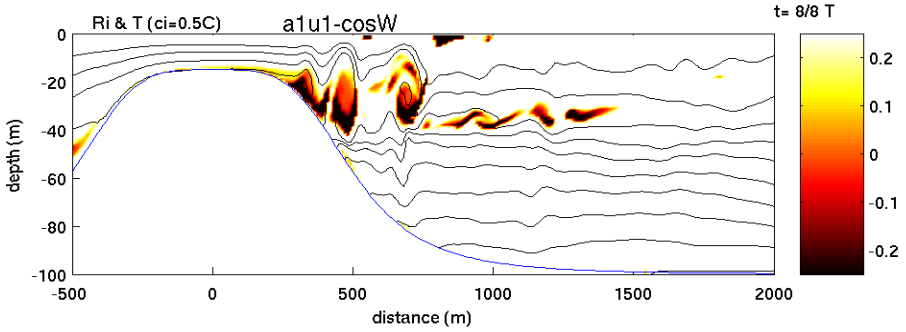
Ri & T (ci=0.5C)
a1u1-cosW
t= 8/8 T
depth (m)
distance (m)
0
-20
-40
-60
-80
-100
-500
0
500
1000
1500
2000
0.2
0.1
0
-0.1
-0.2

8a

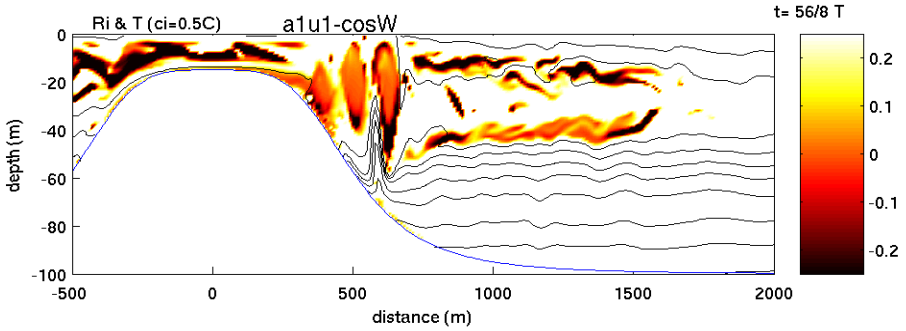
Ri & T (ci=0.5C)
a1u1-cosW
t= 56/8 T
depth (m)
distance (m)
0
-20
-40
-60
-80
-100
-500
0
500
1000
1500
2000
0.2
0.1
0
-0.1
-0.2

8b

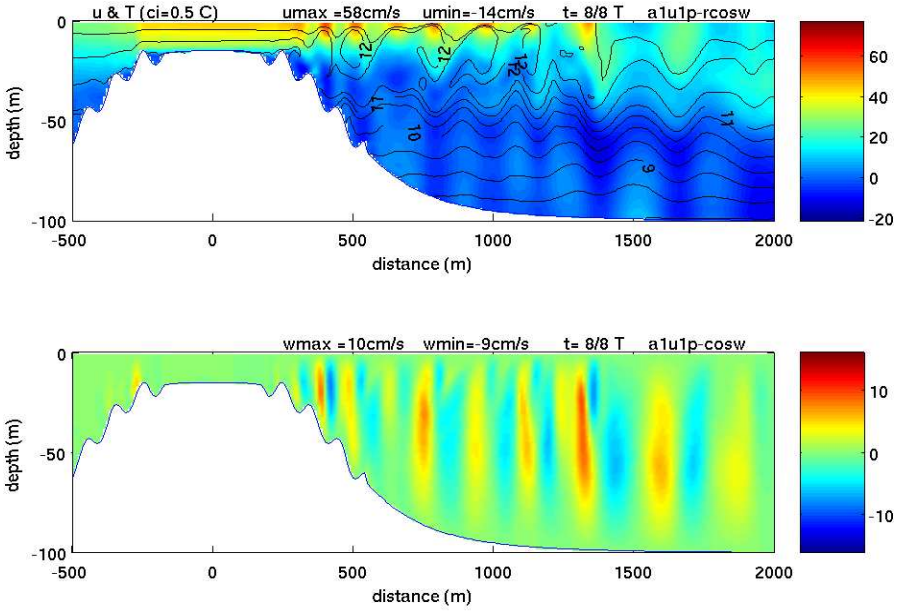
u & T (ci=0.5 C)
umax =58cm/s
umin=-14cm/s
t= 8/8 T
a1u1p-rcosw
depth (m)
distance (m)
wmax =10cm/s
wmin=-9cm/s
t= 8/8 T
a1u1p-cosw
depth (m)
distance (m)

9a

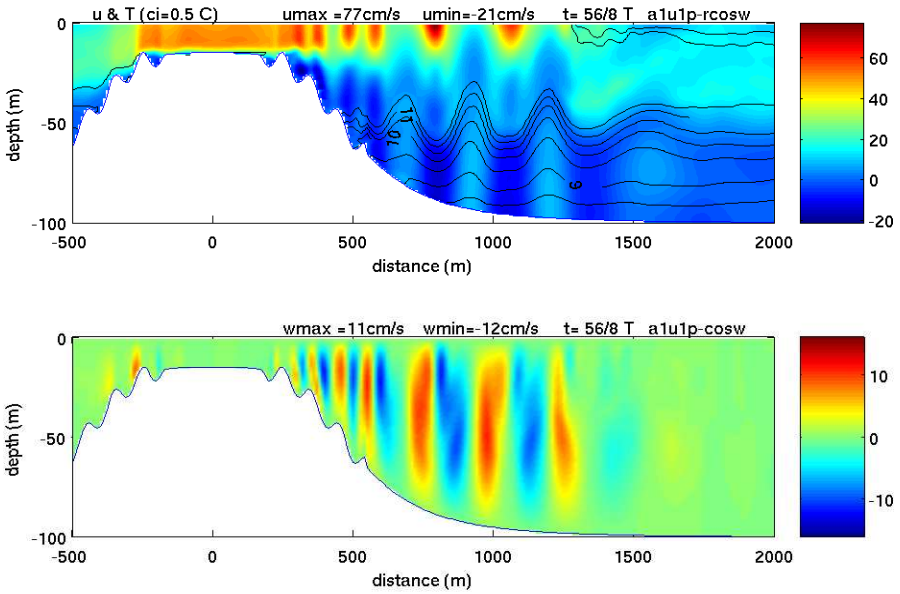
u & T (ci=0.5 C)
umax =77cm/s
umin=-21cm/s
t= 56/8 T
a1u1p-rcosw
depth (m)
distance (m)
wmax =11cm/s
wmin=-12cm/s
t= 56/8 T
a1u1p-cosw
depth (m)
distance (m)

9b

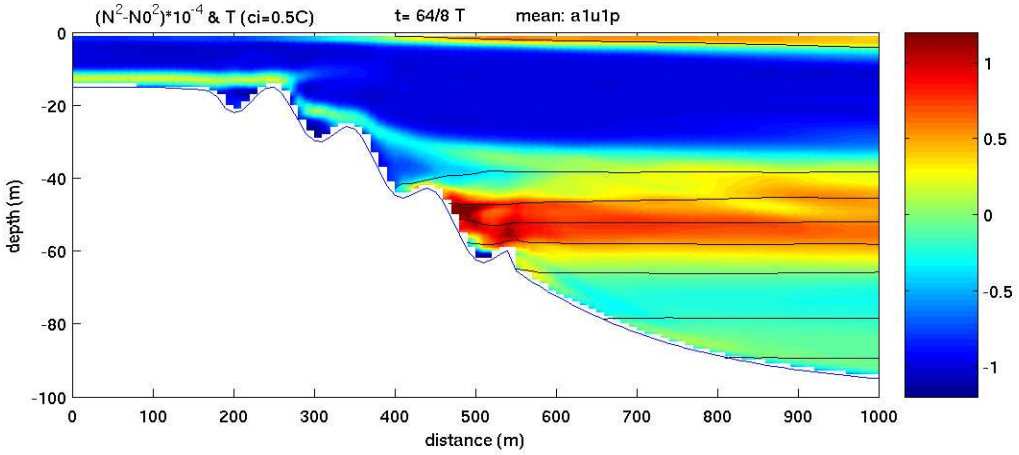
(N2-N02)*10-4 & T (ci=0.5C)
t= 64/8 T
mean: a1u1p
depth (m)
distance (m)
0
-20
-40
-60
-80
-100
0
100
200
300
400
500
600
700
800
900
1000
1
0.5
0
-0.5
-1

9c

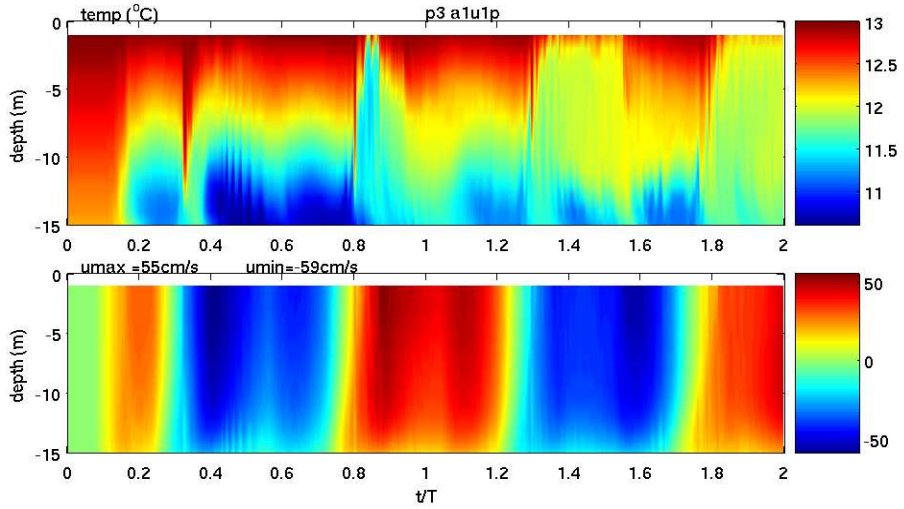
temp (°C)
p3 a1u1p
depth (m)
umax =55cm/s
umin=-59cm/s
t/T

10a

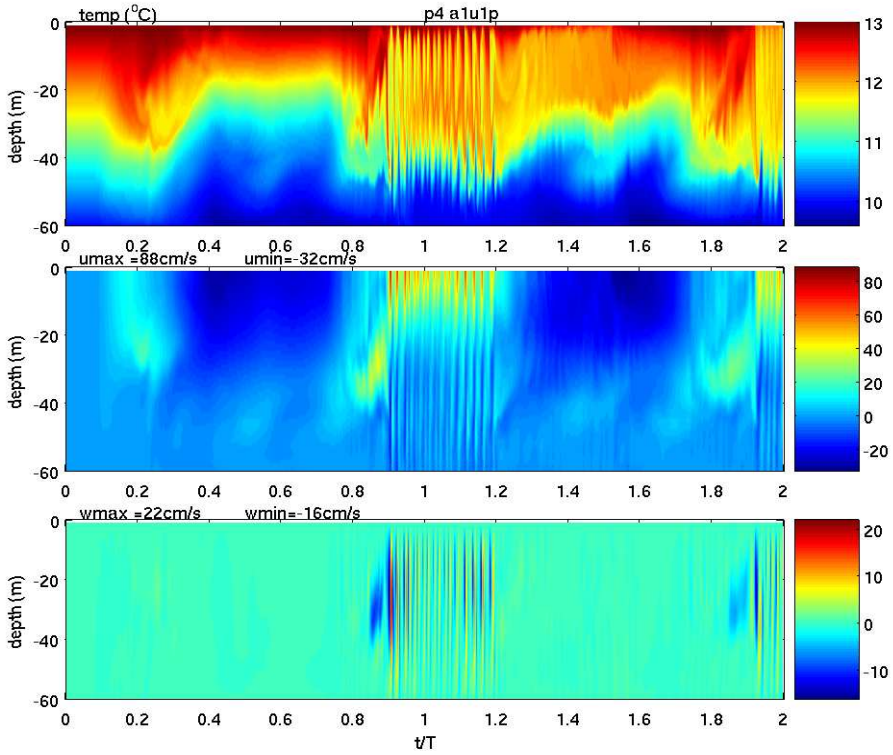
temp (°C)
p4 a1u1p
depth (m)
umax =88cm/s
umin=-32cm/s
wmax =22cm/s
wmin=-16cm/s
t/T

10b

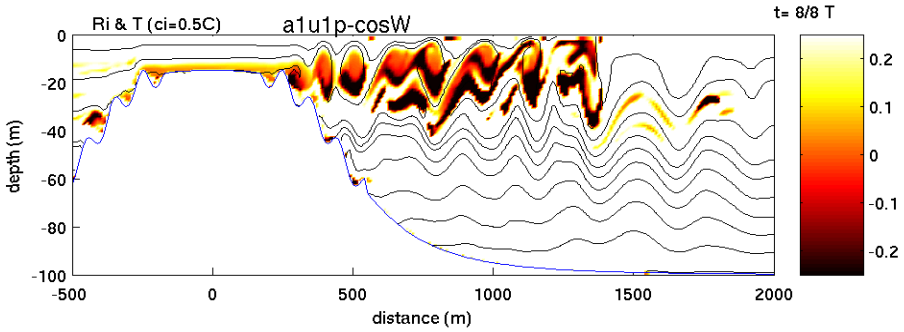
Ri & T (ci=0.5C)
a1u1p-cosW
t= 8/8 T
depth (m)
distance (m)
0
-20
-40
-60
-80
-100
-500
0
500
1000
1500
2000
0.2
0.1
0
-0.1
-0.2

11

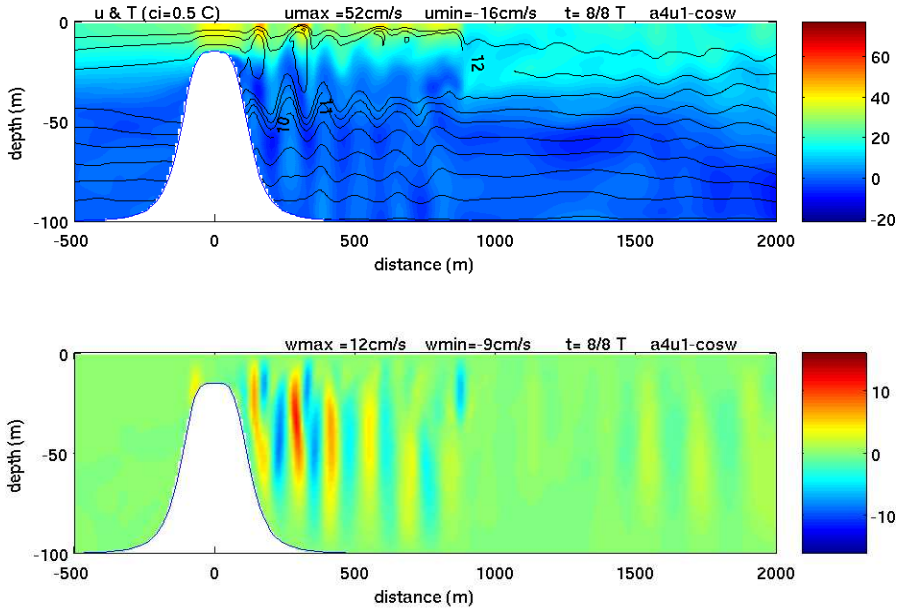
u & T (ci=0.5 C) umax =52cm/s umin=-16cm/s t= 8/8 T a4u1-cosw
depth (m)
distance (m)
wmax =12cm/s wmin=-9cm/s t= 8/8 T a4u1-cosw
depth (m)
distance (m)

12a

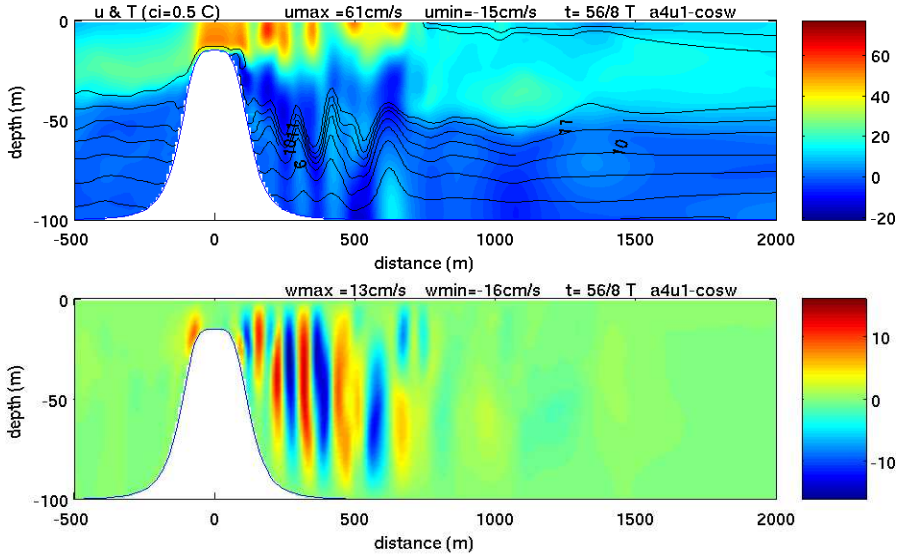
u & T (ci=0.5 C) umax =61cm/s umin=-15cm/s t= 56/8 T a4u1-cosw
depth (m)
distance (m)
wmax =13cm/s wmin=-16cm/s t= 56/8 T a4u1-cosw
depth (m)
distance (m)

12b

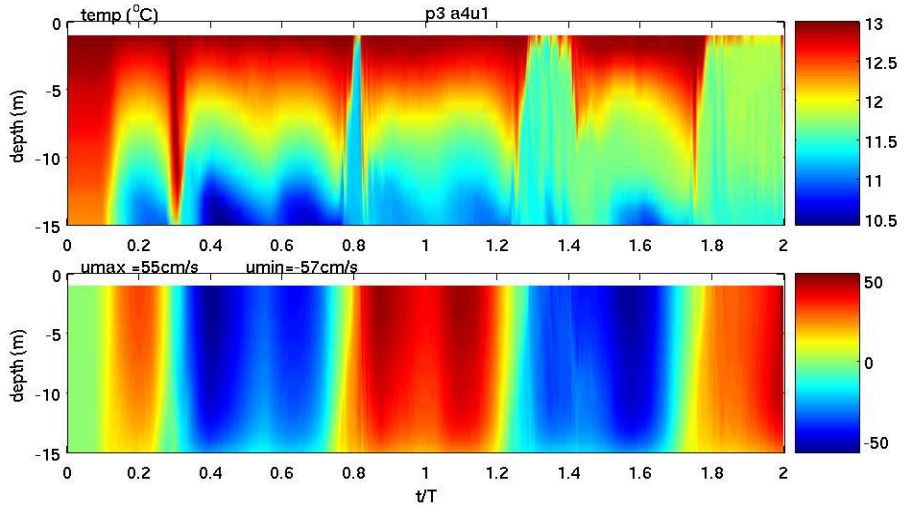
temp (°C)
p3 a4u1
depth (m)
umax =55cm/s
umin=-57cm/s
t/T

13a

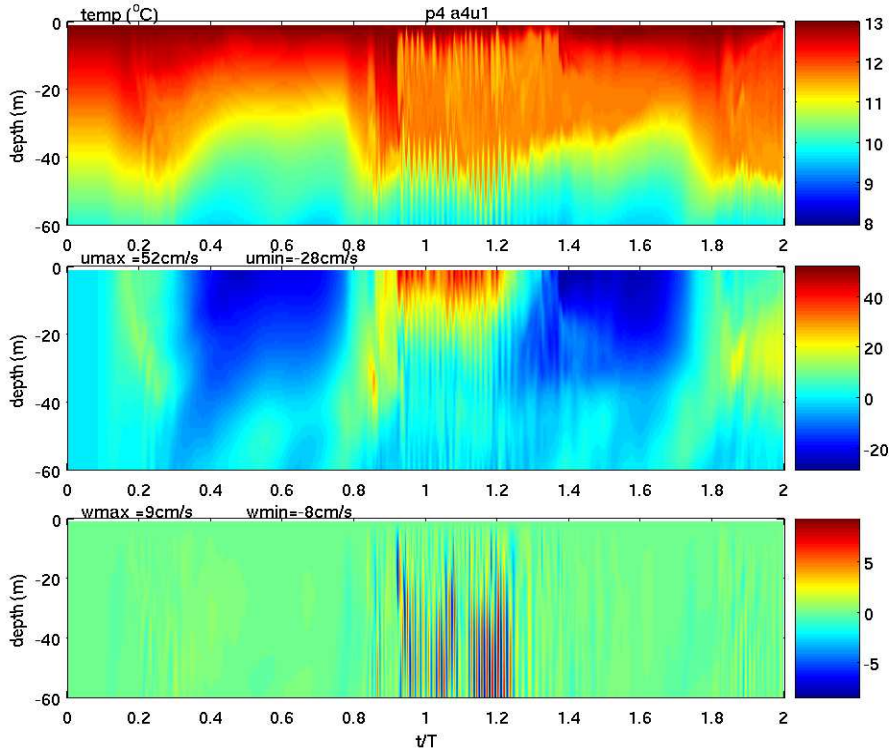
temp (°C)
p4 a4u1
depth (m)
umax =52cm/s
umin=-28cm/s
wmax =9cm/s
wmin=-8cm/s
t/T

13b

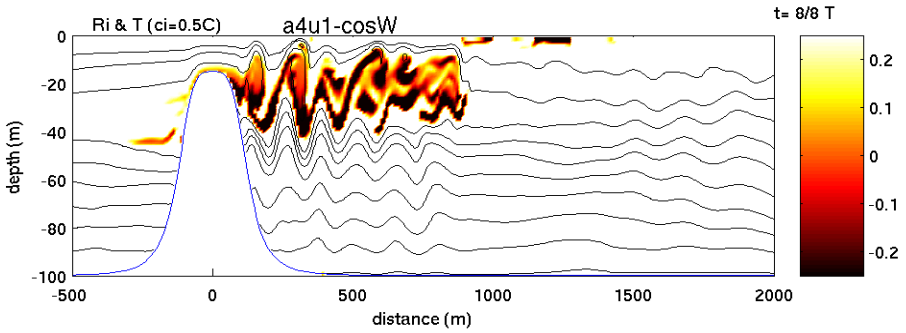
Ri & T (ci=0.5C)
a4u1-cosW
t= 8/8 T
depth (m)
distance (m)
0
-20
-40
-60
-80
-100
-500
0
500
1000
1500
2000
0.2
0.1
0
-0.1
-0.2

14a

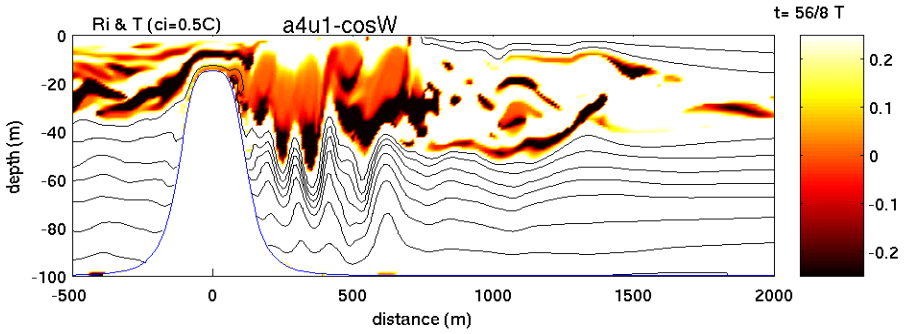
Ri & T (ci=0.5C)
a4u1-cosW
t= 56/8 T
depth (m)
distance (m)
0
-20
-40
-60
-80
-100
-500
0
500
1000
1500
2000
0.2
0.1
0
-0.1
-0.2

14b

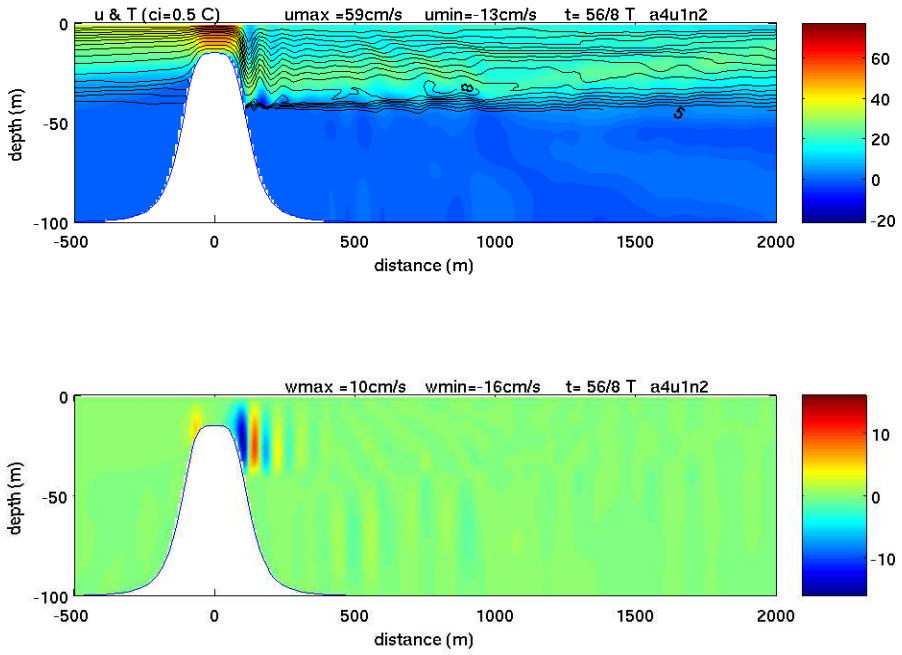
u & T (ci=0.5 C)
umax =59cm/s
umin=-13cm/s
t= 56/8 T
a4u1n2
depth (m)
distance (m)
wmax =10cm/s
wmin=-16cm/s
t= 56/8 T
a4u1n2
depth (m)
distance (m)

15a

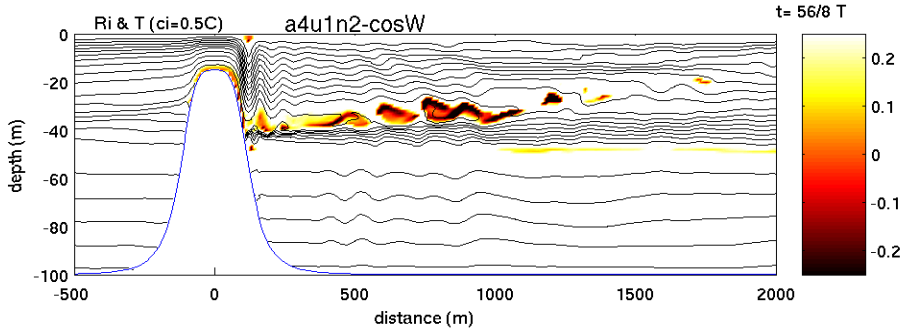
Ri & T (ci=0.5C)
a4u1n2-cosW
t= 56/8 T
depth (m)
distance (m)

15b

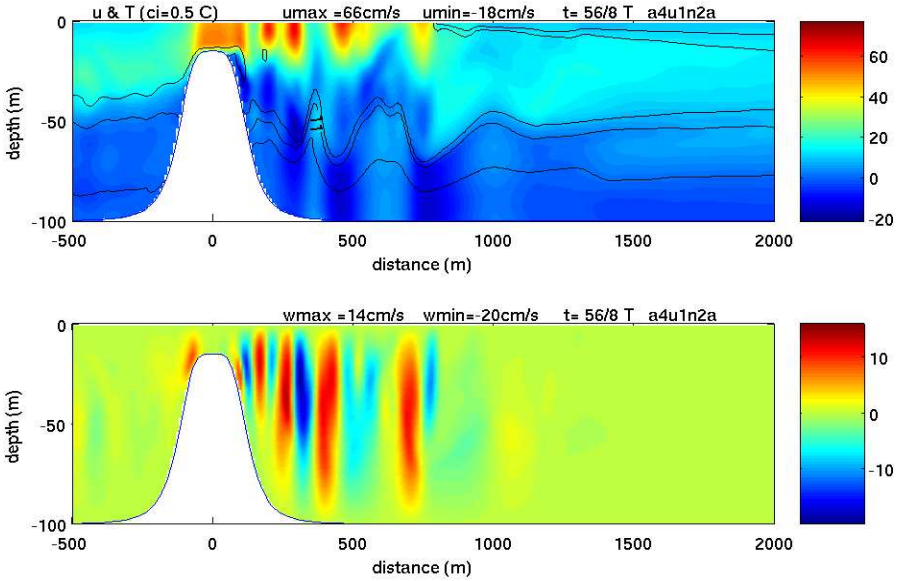
u & T (ci=0.5 C)
umax =66cm/s
umin=-18cm/s
t= 56/8 T
a4u1n2a
depth (m)
distance (m)
wmax =14cm/s
wmin=-20cm/s
t= 56/8 T
a4u1n2a
depth (m)
distance (m)

16a

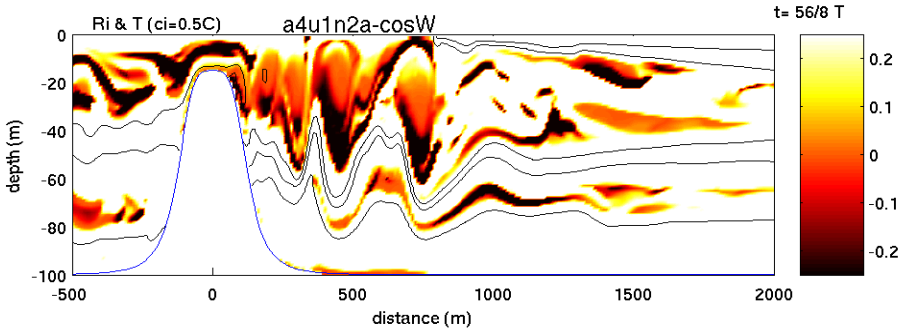
Ri & T (ci=0.5C)
a4u1n2a-cosW
t= 56/8 T
depth (m)
distance (m)

16b